

1 Snow Depth Estimation on Lead-less Landfast ice using Cryo2Ice 2 satellite observations

3 Monojit Saha¹, Julienne Stroeve^{1,2}, Dustin Isleifson¹, John Yackel³, Vishnu Nandan^{1,3}, Jack Landy⁴, Hoi
4 Ming Lam³

5 1Centre for Earth Observation Science, Department of Environment and Geography, University of Manitoba, Winnipeg,
6 Canada

7 2 Department of Earth Sciences, University College London. London, United Kingdom

8 3 Department of Geography, University of Calgary, Calgary, Canada

9 4 Centre for Integrated Remote Sensing and Forecasting for Arctic Operations (CIRFA), UiT The Arctic University of Norway,
10 Tromsø, Norway

11
12 *Correspondence to:* Monojit Saha (saham1@myumanitoba.ca)

13 **Abstract.** Observations of snow on Arctic Sea ice are vitally important for sea ice thickness estimation, bio-physical processes
14 and human-activities. While previous studies have combined CryoSat-2 and ICESat-2-derived freeboards to estimate snow
15 depth over Arctic sea ice, these approaches require leads within the ice pack to estimate the freeboard heights above the sea
16 surface. In regions such as the Canadian Arctic Archipelago (CAA), leads are scarce in winter, posing a significant challenge
17 to estimate snow depth from altimeters. This study is the first assessment of the potential for near-coincident ICESat-2 and
18 Cryosat-2 (Cryo2Ice) snow depth retrievals in a lead-less region of the CAA including validation with in-situ data. In lieu of
19 sea surface height estimates from leads, snow depths are retrieved using the absolute difference in surface heights (ellipsoidal
20 heights) from ICESat-2 and Cryosat-2 after applying an ocean tide correction based on tidal gauges between satellite passes
21 on 29th April 2022. Both the absolute mean snow depths and distributions retrieved from Cryo2Ice were slightly
22 underestimated (2 to 4 cm) when compared to in-situ measurements. All four in-situ sites had snow with saline basal layers
23 and different levels of roughness/ridging which significantly impacts the accuracy of the Cryo2Ice snow depth retrievals.

24 Differences between Cryo2Ice and in-situ snow depth distributions reflect the varying sampling resolutions of the sensors and
25 the in-situ measurements. Cryo2Ice tends to miss snow depths greater than 30 cm, especially around ridges. The results suggest
26 that it might be possible to estimate snow depth over landfast sea ice without leads. However, the observed biases of 2-4 cm
27 likely stem from several factors: (1) discrepancies in sampling resolution between ICESat-2 and CryoSat-2, (2) the CryoSat-2
28 scattering horizon not aligning with the snow-ice interface due to snow salinity, density, and surface roughness, (3) the choice
29 of retracker, and (4) potential errors in the altimeter's tidal corrections. Further investigation is needed to address these issues.
30 Moreover, the proposed methodology for getting snow depth over lead-less landfast sea ice needs to be validated using in-situ
31 datasets in other landfast sea ice regions in the Arctic. ~~Differences in the Cryo2Ice and in-situ snow depth distributions reflected~~

~~the different sampling resolutions between the sensors and the in-situ measurements, with Cryo2Ice missing snow depths greater than 30 cm especially around ridges. Results suggest the possibility of estimating snow depth over lead-less landfast sea ice. However, the observed 2-4 cm biases likely result from a combination of we attribute but attributing a 2-3 cm biases to (1) differences in sampling resolution between ICESat-2 and CryoSat-2/IS2 and CS2, (2) CryoSat-2 CS2 dominant scattering horizon not being at the snow-ice interface due to the impact of snow salinity, density, snow surface roughness, (3) choice of retracker and/or (4) errors in altimeter's tidal corrections require further investigation.~~

1 Introduction

Changes in Arctic sea ice are affecting climate, ecosystems and traditional ways of living and harvesting (Meier and Stroeve, 2022). A critical component of the sea ice cover is its overlying snow cover, which has been challenging to accurately measure by satellites (Webster et al., 2018). Snow acts as an insulator, impacting both the growth and decay of sea ice (Maykut and Untersteiner, 1971). Snow also (1) limits the amount of light penetrating through the sea ice, affecting the timing of sea ice algae growth (Mundy et al., 2005); (2) contributes to the amount of freshwater discharged to the ocean, affecting its budget (Andersen et al., 2019); and (3) affects the heat exchange between the atmosphere and the sea ice (Andreas et al., 2005).

Using monthly composites of airborne laser and radar altimeter data collected during the Laser-Radar Altimetry (LaRA) mission over sea ice around Svalbard, Leuschen et al., 2008, suggested snow depth could be retrieved by differencing freeboards, though there was a lack of in-situ ground truth to validate results. Following this, studies have differenced coincident satellite radar (CryoSat-2; hereafter CS2) and laser (ICESat-2; hereafter IS2) altimeter freeboards to estimate pan-Arctic (e.g. Kwok and Markus, 2018; Kwok et al., 2020) and Antarctic snow depth (Kacimi and Kwok, 2020). However, significant uncertainties remain related to (1) differences in electromagnetic frequencies and spatial resolution (Fons et al., 2021); (2) whether or not the CS2 Ku-band radar returns originate from the snow/ice interface, which has been contested even for a dry and cold (below freezing) snow pack (Willatt et al., 2023, 2011; Nandan et al., 2017; de Rijke Thomas et al., 2023); (3) the influence of surface roughness over different length scales on the laser and radar waveforms (Landy et al., 2019); and (4) spatial heterogeneity of snow distributed over sea ice.

Earlier studies also faced challenges of having different orbits for CS2 and IS2, limiting the number of crossover points (Kwok & Markus, 2018). Kwok and Markus (2018) made a case for adjusting the CS2 orbit to achieve more overlaps with IS2, thereby improving both spatial and temporal coincidence. As part of the Cryo2Ice campaign, the CS2 orbit was raised by ~900 meters in August 2020 to significantly increase the amount of crossovers with IS2 (ESA, 2020). This realignment means that once in every 19 CS2 (20 IS2) cycles, the two ground tracks nearly align for hundreds of kilometers over the Arctic ~~providing new opportunities to improve and validate snow depths retrieved by combining laser and radar freeboards. However, Freedensborg Hansen et al., (2024) provides the first analysis of Cryo2Ice along-track snow depths retrieved using the freeboard differencing method over 7 km segments and reports uncertainties of 10-11 cm.~~

63 ~~With the Cryo2Ice campaign, new opportunities have emerged to improve and validate snow depths retrieved by combining~~
64 ~~laser and radar freeboards. previously While~~ [Fredensborg Hansen et al. \(2024\)](#) ~~took advantage of the Cryo2Ice campaign to~~
65 ~~retrieve along-track snow depths along 7-km segments. In their study, they compared~~ [Freesborgsen Hansen et al \(2024\)](#) ~~have~~
66 ~~compared the derived Cryo2Ice snow depths over larger segments (7-km long segments) and used~~ ~~against snow depth products~~
67 ~~from passive microwave, snow models or climatologies and found uncertainties of 10-11cm.;~~
68 [This study is the first comparison of Cryo2ice snow depths to in-situ snow depth retrievals over landfast ice, evaluating](#)
69 [retrievals along both 300-meter and 1-km/1-kilo-meter segments.](#) This study [also](#) provides the first high-resolution in-situ
70 validation of snow depths retrieved along coincident Cryo2Ice tracks ~~on the 29th of April 2022 (29-04-2022)~~ near Cambridge
71 Bay, Nunavut in the Canadian Arctic Archipelago (CAA). The CAA is a region with significantly different bathymetry and
72 icescape than the Central Arctic (Galley et al., 2012). Sea ice in the CAA is landfast ice for the majority of the year (6 to 8
73 months) (Melling, 2002), and exhibits minimal ice drift (Galley et al., 2012), making it easier to match up IS2 and CS2 tracks.
74 On the other hand, the tidal amplitudes within the shallow bathymetry of the CAA are larger than in the open ocean; posing
75 an additional challenge compared to validation studies in the Central Arctic Ocean. However, the most prominent challenge
76 pertains to the lack of open water for estimating the local sea surface height (SSH) needed to reference the freeboards. Landfast
77 ice grows along the narrow channels in the CAA and often lacks leads for several hundred kilometers (Galley et al., 2012).
78 Therefore, assuming IS2 and CS2 are viewing the same landfast ice, the variation in SSH due to tidal variations must be known
79 and corrected for between the two sensors. Our objective is to develop an approach to combine IS2 and CS2 along-track data
80 in regions where the local SSH estimate is not readily available from satellite observations. The along-track Cryo2Ice retrieved
81 snow depths are then validated using near-coincident in-situ snow depth observations. We further use in-situ snow property
82 observations and satellite estimates of the surface roughness to examine the drivers of CS2 and IS2 height variability. Finally,
83 the sources of bias in the retrieval process and major challenges are discussed.

84 **2 Data and Methods**

85 **2.1 ICESat-2 (IS2)**

86 The Advanced Topographic Laser Altimeter System (ATLAS) is the photon counting LiDAR system onboard ICESat-2.
87 ATLAS emits low-energy 532 nm (green) pulses in three two-beam pairs which have a cross track spacing of 3.3 km between
88 each pair with intra-pair spacing of 90 meters. The laser has a footprint size of 11 meters (Magruder et al., 2020). Detailed
89 specifications can be found in Neumann et al., (2019).

90 In this study, the uncorrected ATL07 Sea Ice Height Release Version 6 available from the National Snow and Ice Data Centre
91 (<https://nsidc.org/data/atl07ql/versions/6#anchor-2>) which are computed directly from ATL03 photon heights are used. ATL07
92 contains sea surface and sea ice heights derived from ATL03 photon heights that were aggregated into segment lengths
93 consisting of 150 photons, resulting in variable along-track lengths over which these photos are accumulated. In the uncorrected
94 ATL07 product, sea ice heights within the 25 km land-buffer are included despite low confidence in the geophysical corrections

95 close to land (Kwok et al., 2023). The IS2 strong beam (gt2l) (referred to as IS2 2l) from ATL07 is used after assessing all
96 three strong beams. The IS2 2l was ~1500 metre from the CS2 point of closest approach whereas beams 1l and 3l were ~2200
97 metre and ~4500 metre away, respectively.

98 The geophysical corrections applied to the ATL07 data are summarized in Table A1. Each correction is time-varying and has
99 different impacts on the retrieved IS2 heights. Ocean tide corrections are provided every hour and can vary from -62 cm to
100 +62 cm; the largest among the different geophysical corrections applied. The ocean tide corrections are obtained from the
101 Global Ocean Tide Model 4.8 (GOT 4.8) (Kwok et al., 2021), which provides tidal predictions for all regions of the globe
102 based on the assimilation of data from satellite altimetry and tide gauge measurements into a tidal model.

103 **2.2 CryoSat-2 (CS2)**

104 The SAR Interferometric Radar Altimeter (SIRAL) is the primary instrument on board CryoSat-2, which is a combination of
105 a pulse-limited radar altimeter along with a Synthetic Aperture Radar (SAR) Interferometer system (SARIn). SIRAL operates
106 at Ku-band (13.575 GHz) and in three different modes with along-track sampling resolution of around 300 m and across-track
107 resolution of 1600 m (ESA, 2013). Cryosat-2 operated in the SARIn mode in the CAA during the study period. Here we use
108 the CS2 Level 2 Baseline E products available through the European Space Agency's EO-CAT web explorer
109 (<https://eocat.esa.int/>). The CS2 Level 2 sea ice heights are re-tracked using the University College London (UCL) retracker
110 (Tilling et al., 2018) which assumes a threshold (70%) on the first peak for diffuse echoes representing the mean elevation of
111 the snow/sea ice interface within the footprint. This fixed threshold retracker is used in the CS2 Baseline E level product over
112 sea ice floes in the SAR/SARIn mode.

113 Tidal corrections (ocean, long-period equilibrium, ocean loading, solid earth and geocentric polar) are included in the Level 2
114 Baseline E Cryosat-2 SAR/SARIn product (Table B2). The ocean tide, long-period equilibrium tide and ocean loading tide
115 corrections used are retrieved from the Finite Element Solution 2004 Ocean Tide Model (FES 2004) (Cryosat-2 Product
116 Handbook). The ocean tide corrections typically range from ± 50 cm.

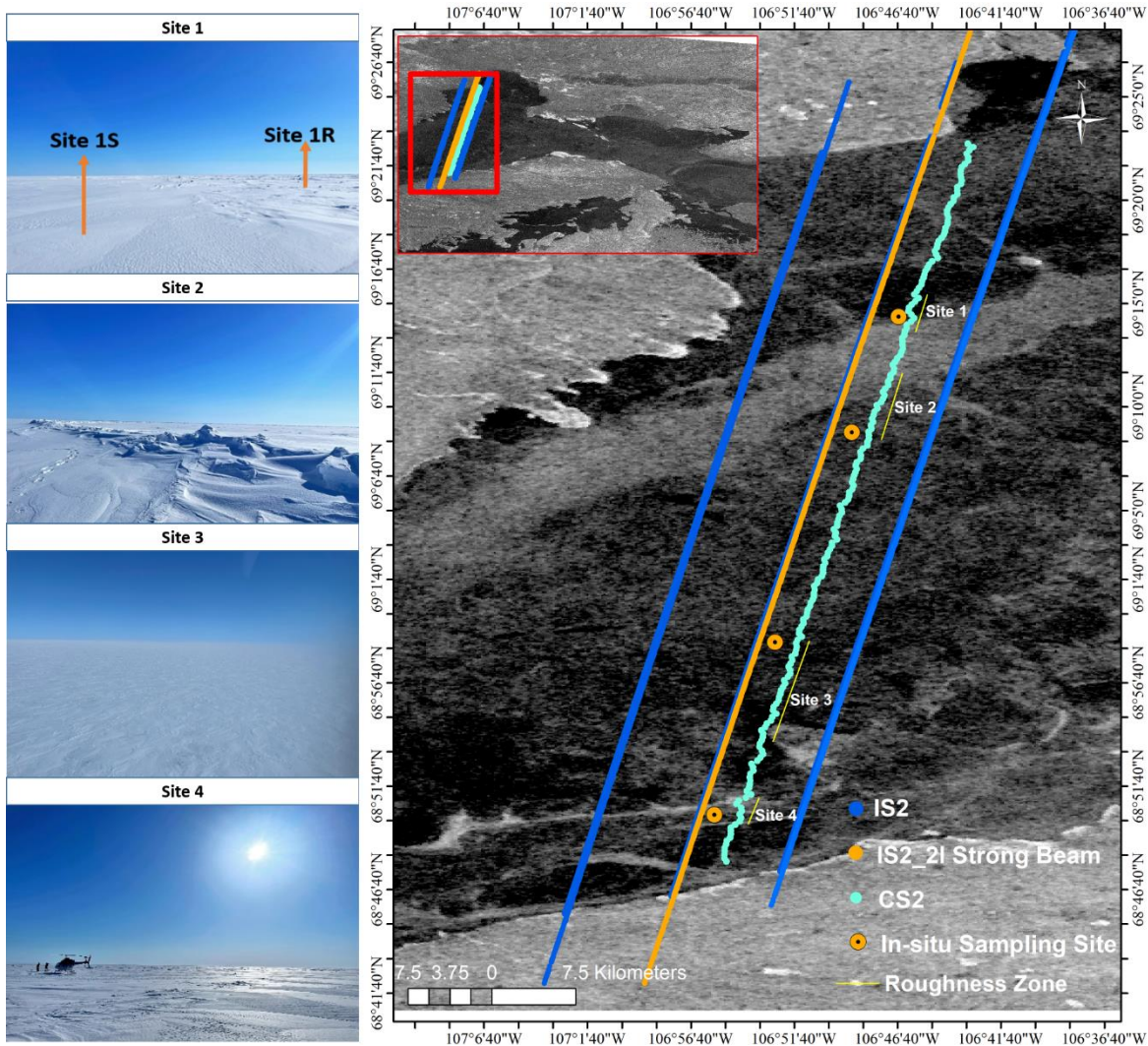
117 **2.3 Sentinel-1 SAR**

118 Synthetic Aperture Radar (SAR) imagery from European Space Agency's Sentinel-1 satellite was used in this study in
119 conjunction with IS2 and CS2. Sentinel-1 provides dual-polarization SAR data which is available through the Google Earth
120 Engine platform (https://developers.google.com/earth-engine/datasets/catalog/COPERNICUS_S1_GRD). The Sentinel-1
121 GRD files had already been pre-processed with the following corrections: GRD border noise removal, thermal noise removal,
122 radiometric calibration and terrain correction. For this study, the cross-polarized VH backscatter was obtained from May 5th,
123 2022. The backscatter values were then converted to dB.

124

125 **2.4 Field Measurements**

126 The study site comprised a 75 km long NNE-to-SSW transect across Dease Strait ($69^{\circ}26'58.02''\text{N}$ $106^{\circ}41'57.25''\text{W}$ to
127 $68^{\circ}46'42.48''\text{N}$ $106^{\circ}55'52.10''\text{W}$) (Figure 1), ~70 km west of Cambridge Bay, NU. This region connects Coronation Gulf and
128 Queen Maud Gulf of the Kitikmeot Sea and is a part of the southern route of the Northwest Passage (Xu et al., 2021). Dease
129 Strait is relatively shallow (maximum depth ~ 100 meters), and its narrow channel is covered by landfast ice normally between
130 November and mid-July (Galley et al., 2012). CS2 and IS2 coincident tracks were identified using the CS2 and IS2 Coincident
131 Data Explorer (<https://cs2eo.org/>) (Ewart et al., 2022). The tracks were ~1.5 km apart and passing by within 77 minutes of
132 each other (Figure 1).



133
134 **Figure 1** Map shows the Cryosat-2 Points of Closest Approach (POCA) locations, IS2 2l Strong Beam and other IS2 beam, in-situ
135 sampling locations and identified roughness zones. The background contains Sentinel-1 HH-pol SAR imagery. Site photos show the
136 variation in snow roughness.

137 In-situ snow depths were collected at four different sites (Sites 1-4) ranging from smooth, rough and mixed sea ice roughness
138 zones. The transects were set considering wind direction as well as the sea ice surface features for each site. The sampling
139 strategy was to ensure coverage of the Cryo2Ice along-track and across-track directions, taking into consideration the
140 prevailing wind direction and different representative roughness features. At Site 1, two L-shaped transects representing the
141 rough and smooth sea ice zones were conducted (Figure D1 (a)). For Site 2, two different L-shaped transects were conducted
142 to sample both the ridged ice areas as well as the smoother ice further away from the ridges (Figure D1(b)). For Sites 3 and 4
143 which had wider regions of smooth and rough sea ice respectively, two L-shaped transects were conducted (Figure D1 (c) &
144 (d)). Based on Sentinel-1 SAR and field reconnaissance, Site 1 was classified as a rough and smooth sea ice transition zone;
145 Site 2 was a thin snow zone with significant ridging; Site 3 was a smooth sea ice zone with extensive areas of thin snow; and
146 Site 4 was a rough sea ice site with extensive areas of thick snow. All sites were located equidistant between the IS2 strong
147 beam and CS2 track to ensure the highest likelihood that snow depth sampling was representative of both sensors. The snow
148 depth sampling direction was determined according to distinctive roughness features at individual sites, ensuring sufficient
149 sampling distance in both the along- and across-track directions, representative of the prevailing east-southeast wind direction
150 (ECCC, 2022) and snow dune pattern (Moon et al., 2019). Snow depth was surveyed using Snow-Hydro's automated snow
151 depth magnaprobe, which has an accuracy of ± 0.3 cm on level sea ice and snow (Strum and Holmgren, 2018). The magnaprobe
152 was reassembled and re-calibrated before each sampling effort to avoid instrument bias. Sampling was conducted by a single
153 person to avoid variations in instrument handling and to maintain constant intervals between samples.

154 All four sites were surveyed on 01-05-2022 within 48 hours of the ICESat-2 and CryoSat-2 pass on 29-04-2022. The sites
155 were accessed via helicopter and no sampling was conducted within 200 meters of the helicopter landing zone to avoid snow
156 redistribution during landing. While the sampling interval was initially set at 5 m intervals to ensure spatial heterogeneity and
157 to avoid spatial autocorrelation of the sampled snow depth values following Iacozza and Barber (1999), the sampling interval
158 ranged between 2 to 3.8 m during the field sampling for all sites. There was no precipitation recorded during the sampling
159 period, nor during the time interval between the CS2 and IS2 overpasses. Furthermore, high pressure dominated the region
160 between 26-04-2022 and 04-05-2022 (ECCC, 2022) causing light surface winds. As such, snow redistribution between CS2
161 and IS2 overpasses and in-situ sampling was negligible. The air temperature varied between -11.7°C and -14.1°C during the
162 sampling as measured at the Cambridge Bay, land-based meteorological station.

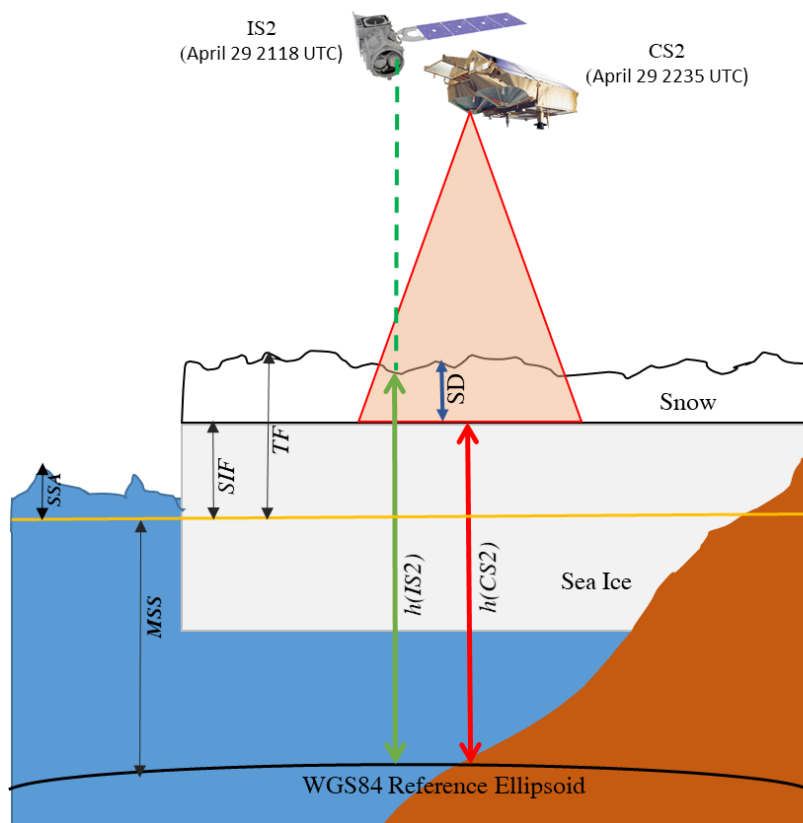
163 Snow geophysical properties including snow salinity and density were sampled from all four sites. Snow temperature was not
164 measured because the temperature probe would not calibrate quickly enough between the short helicopter landing durations.
165 For Site 1, two pits were sampled, one for the rough sea ice (Site 1a) and one for the relatively smooth sea ice zone (Site 1b).
166 Single pits were excavated at the other three sites. Snow density was measured using a 66 cm^3 ($2 \times 5.5 \times 6$ cm) density cutter
167 at 2 cm intervals and weighed in the lab. After, weighed samples were melted at room temperature for snow salinity
168 measurement using a Cole-Parmer C100 Conductivity Meter (accuracy of $\pm 0.5\%$). Sea ice thickness and freeboard at each
169 site was measured using a freeboard tape to an accuracy of 0.5 cm.

170 2.5 Estimating Snow Depth from Cryosat-2 and ICESat-2

171 Kwok et al (2020) calculates snow depth (SD) as the difference between IS2-derived total freeboard (snow + ice) and CS2-
172 derived radar freeboard (CS2). Freeboard heights are computed relative to the instantaneous sea surface height interpolated
173 from sea surface measurements from along-track leads (Kwok et al., 2020; Ricker et al., 2014). The CS2 radar freeboard is
174 additionally adjusted for reduced Ku-band propagation speed through snow. While this approach has been applied to the
175 Cryo2Ice campaign within the central Arctic ([Fredensborg Hansen ~~osberg~~](#) et al., 2024), freeboards require accurate estimation
176 of the sea surface height which is dependent on the availability of leads within a reasonable distance (10's of km) along both
177 the IS2 and CS2 track. No leads were detected along the portion of the IS2 and CS2 tracks in our study area and therefore the
178 sea surface height could not be reliably estimated. Therefore, we modified the approach used in Kwok et al., (2020) to instead
179 use the absolute sea ice heights measured from IS2 ATL07 (h_{IS2}) and CS2 (h_{CS2}) referenced to the WGS84 ellipsoid to
180 estimate SD (Figure 3). SD can be calculated as the freeboard differences under the assumption that Ku-band penetrates to the
181 snow/ice interface

$$182 \quad SD = \frac{h_{IS2} - h_{CS2}}{\eta_s}, \quad (1)$$

183 Where η_s is the refractive index of Ku-band microwaves which compensates for the propagation delay through the snow pack
184 (Kwok et al., 2020). The refractive index is calculated using ($\eta_s = (1 + 0.51\rho_s)^{1.5}$) (Ulaby et al., 1986), where the in-situ bulk
185 snow density (ρ_s) measured from the field is used. The average snow density from all four sites is used to compute snow depth
186 for the entire track (Figure 8) while snow densities from each site are used to compute SD from corresponding portions of the
187 Cryo2Ice track (Figure 5).



188

189 **Figure 2** Schematic showing the calculation of snow depth (SD) from ICESat-2 and Cryosat-2 over sea ice. The diagram illustrates
 190 the representative heights for the sea surface anomaly (SSA), mean sea surface (MSS) in yellow, sea ice freeboard (SIF) and total
 191 freeboard (TF). SD is shown with the blue arrow, IS2 surface height ($h(IS2)$) is shown with the green arrow and CS2 surface height
 192 ($h(CS2)$) is represented by the red arrow. Land is orange.

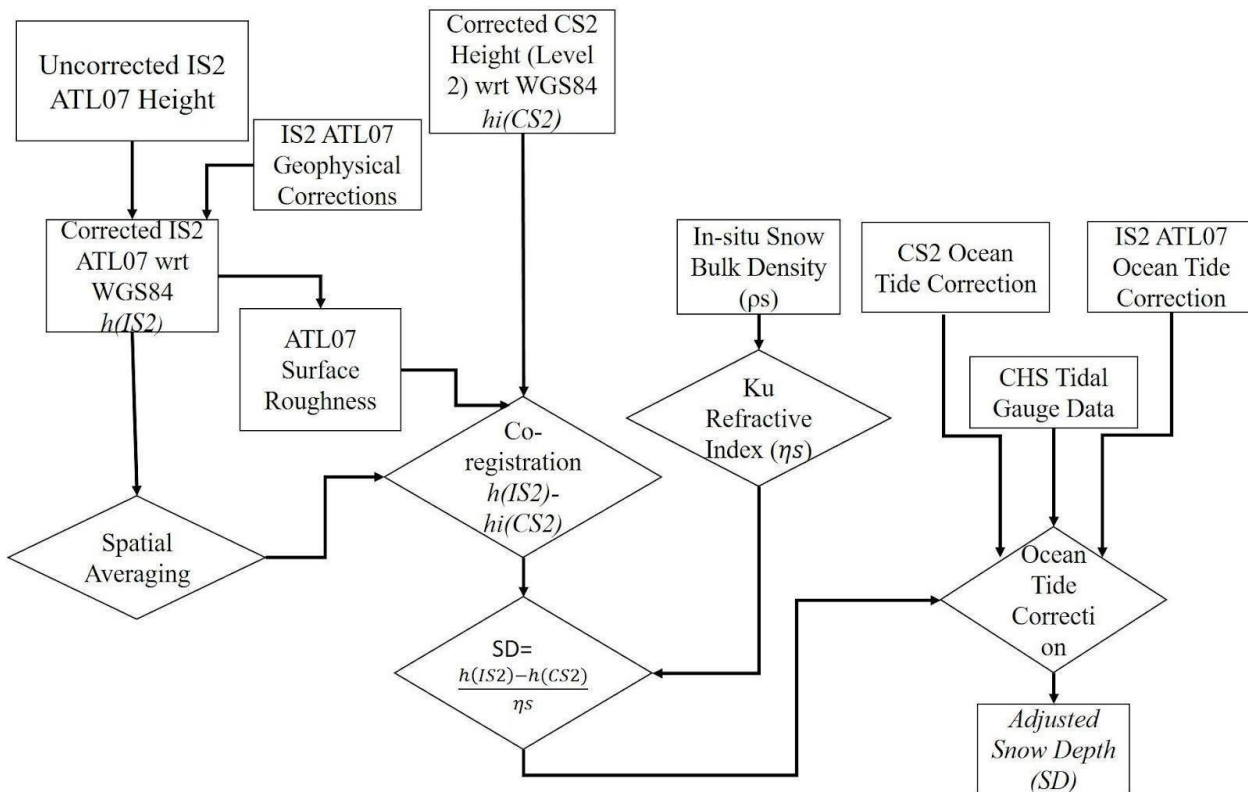
193 2.6 Data Processing

194 The uncorrected IS2 ATL07 heights ($h(IS2)$) are referenced to the WGS84 ellipsoid which is also consistent with the CS2
 195 heights (Figure 2). In our processing of the ATL07 data we apply the following geophysical corrections which are contained
 196 within the IS2 ATL07 product: ocean tide correction, long-period equilibrium tide and inverted barometer correction. We do
 197 not apply the mean sea surface (MSS) since it is based on decadal averages and therefore is not representative of the variation
 198 of sea surface heights within the 77 minute interval between the IS2 and CS2 passes. The geophysical corrections included
 199 within the CS2 data product are applied to the CS2 L2 sea ice heights. However, as mentioned previously the two products do
 200 not have the same tidal corrections.

201 Further, there is limited confidence in these individual geophysical corrections closer to land. The tides varied over a range of
 202 ~ 6.0 cm in Dease Strait in between the two passes based on the tide gauge data, so it was crucial to check if the tidal corrections
 203 contained within the products accurately accounted for tide differences in the ~ 77 minutes between passes. Therefore, after

204 comparing the geophysical correction as explained in Section 2.6, an ocean tide correction factor is applied to the Cryo2Ice
 205 snow depths.

206 Since IS2 has a smaller footprint (Section 2.1 and 2.2), the IS2 ATL07 geolocated heights were averaged to be spatially
 207 congruent with the CS2 footprint giving snow depths estimates in the maximum along-track resolution of 300 m. Here, the
 208 IS2 photons are first averaged over 300 m length segments to match the along-track CS2 footprint and then co-registered based
 209 on the distance to the closest CS2 Point of Closest approach. Similarly, to reduce the impact of CS2 noise as explained later
 210 in Section 4.3 , the snow depths are also computed over 1-km. Therefore, each CS2 point is co-registered to the closest 300
 211 metre ATL07 height segment. Snow depths computed from the IS2 and CS2 height differences were estimated following
 212 Equation (1), and subsequently adjusted with the ocean tidal correction. ~~In order to identify the extent of spatial~~
 213 ~~heterogeneity in the retrieved snow depths from Cryo2Ice, the Moran's I test (Moran,1948) is performed to test the level of~~
 214 ~~spatial autocorrelation. The semi variogram analysis of the in-situ snow distribution shows that the snow depth values are~~
 215 ~~correlated within a lag distance of ~1 kilometer. Therefore, to~~ compare snow distributions representative of each sampled field
 216 site (S1 to S4), snow depth is compared over similar roughness zones. Roughness zones corresponding to each Site are defined
 217 as a portion of the CS2/IS2 track which had IS2 surface roughness within one standard deviation of the IS2 derived surface
 218 roughness directly adjacent to the in-situ sampling site (Figure 1). The Cryo2Ice-derived snow depth corresponding to each
 219 roughness site was then compared against the in-situ snow distribution from the sampling sites.



221 **Figure 3 Methodological workflow for retrieving snow depth (SD) from CS2/IS2 co-registered averaged ATL07 (h (IS2)) and**
222 **Cryosat-2 heights (h (CS2)) are subtracted following Equation 1. The differenced product is located at the Point of Closest Approach**
223 **(POCA) of each CS2 footprint. The differenced product is then adjusted with the refractive index (η_s).**

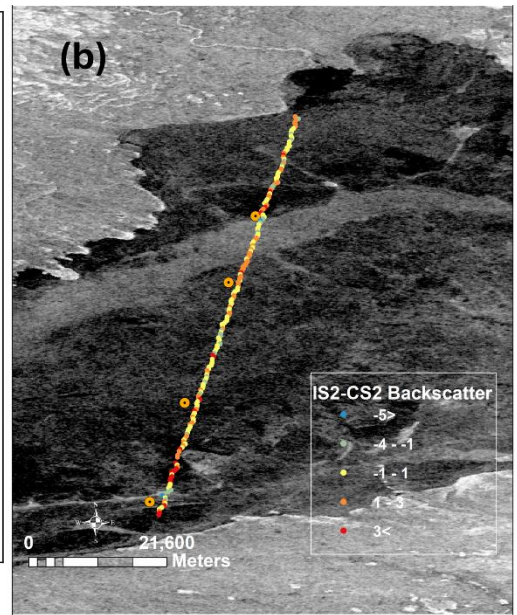
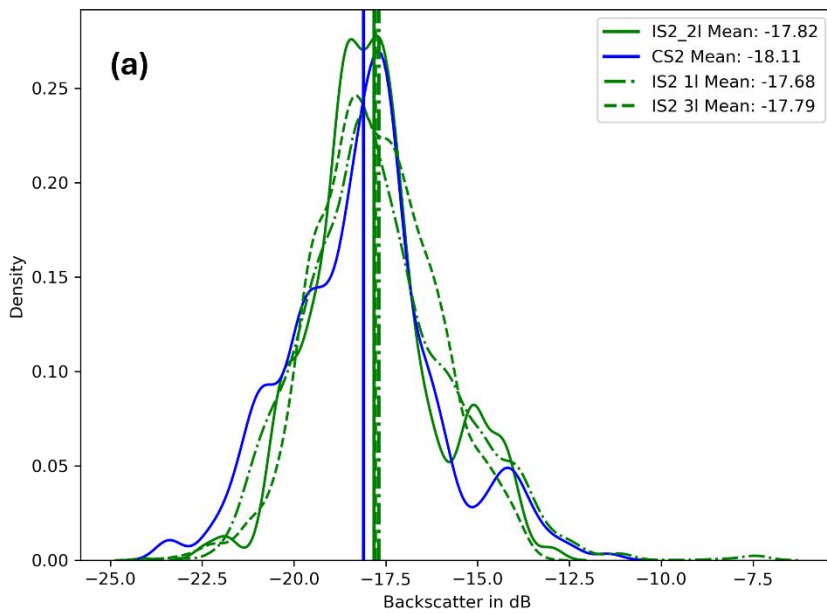
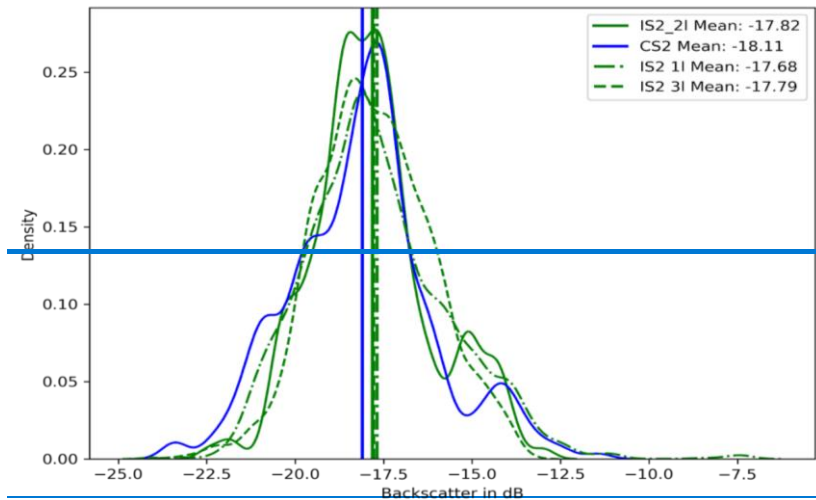
224 **2.7 Adjusting for Sea Surface Height Variation**

225 Assuming IS2 and CS2 are viewing the same landfast ice, any variation in sea surface height over the short 77 minute interval
226 between tracks is assumed to be due to tidal variations. The long-period equilibrium tide and ocean-tide with the inverted
227 barometer corrections were compared between the sensors to identify differences between them. As mentioned earlier,
228 different ocean tide corrections are applied to CS2 and IS2, with values ranging between +/-50 cm in CS2 and +/-62 cm in IS2
229 (Kwok et al, 2021, Cryosat-2 Product Handbook), and these have the most significant impact on the height retrievals (Figure
230 C1, See Figure S1 in Bagnardi et al., 2021)) . Ideally, the ocean tide correction applied to IS2 and CS2 should account for the
231 true variation in SSH due to local tides between the data acquisition passes. Although sea ice significantly dampens tides
232 (Rotermund et al., 2021), tidal fluctuations, in this case the tidal corrections were found to be non-negligible. We compared
233 the average ocean tide corrections to local tidal gauge predictions from the Canadian Hydrographic Service (CHS)
234 (<https://tides.gc.ca>) which are based on real-time and historical tidal gauge measurements from the Cambridge Bay station.
235 The CHS dataset provides instantaneous tidal variations at the CB station every 15 minutes with six observations between the
236 IS2 and CS2 passes. The difference in ocean tidal corrections between the IS2 and CS2 pass was 7.9 cm on average along the
237 track whereas the difference in water level was 6.0 cm according to the CHS data. The difference in height between IS2 and
238 CS2 was therefore adjusted by a single value of 1.9 cm before the snow depths were computed (Figure 3) and this value then
239 represents a systematic uncertainty on the final snow depth estimates.

240 **2.8 Evaluating Other Sources of Uncertainties**

241 One of the critical assumptions is that IS2 and CS2 tracks are roughly coincident i.e. both tracks are measuring roughly the
242 same snow despite their reference ground tracks being ~1.5 km apart. To test this assumption, Sentinel-1 SAR VH backscatter
243 was characterized across both the IS2 and CS2 reference ground tracks. The sentinel-1 backscatter is sensitive to surface
244 roughness which roughly corresponds to the snow depths along-track (Cafarella et a., 2019). Therefore, the Sentinel-1
245 backscatter which is used to compare the backscatter profiles along IS2 and CS2 tracks to determine if they are similar and
246 therefore are seeing similar snow depth distributions. Given that IS2 has three different strong beams (IS2 11,21 and 31), we
247 compare the SAR backscatter across all three tracks and compare it to the SAR backscatter along the CS2 track. We notice
248 that along the IS2 21 track the SAR backscatter shows the most similar backscatter distribution as along the CS2 track (Figure
249 4(a)). This also aligned with the fact that the IS2 21 beam was the closest (~1.5 km) from the CS2 Points of Closest Approach
250 (POCA) and therefore would see the most similar snow distributions. Therefore, the IS2 21 was considered for the subsequent
251 Cryo2Ice snow depth calculations. The SAR pixels intersecting with the IS2 and CS2 track were used to calculate the mean
252 backscatter along each track. The mean difference in SAR backscatter was -0.3 dB, less than 1 standard deviation of the
253 backscatter of each track (Figure 4 (a)). Since both the tracks have similar backscatter, the assumption that they are coincident

254 and observing snow packs with the same distribution is likely valid. Additionally, the difference in the point-to-point
 255 backscatter between IS2 and CS2 was also calculated to assess whether the difference in backscatter is consistent throughout
 256 the track (Figure G1). We see that the average difference in backscatter between the collocated points is within ± 1 dB. The
 257 average difference in backscatter between IS2 and CS2 is 0.9 dB. Since both the tracks have similar backscatter, the assumption
 258 that they are coincident and observing snowpacks with the same distribution is likely to be valid in most cases.
 259
 260



263 **Figure 4 (a)** Sentinel-1 Backscatter in dB obtained from all the strong beams of IS2 (IS2 1I, 2I and 3I) and CS2 track locations. The
 264 Sentinel-1 VH backscatter from 05-05-2022 is used for extracting backscatter along both the tracks to assess whether the observed

265 snow distribution is similar (b) Spatial dDistribution of the Sentinel-1 backscatter between IS2 and CS2 tracks, shown differences
266 in backscatter between IS2 and CS2 on ~~retrieved from collocated Sentinel-1 image from 5th May 2023~~.

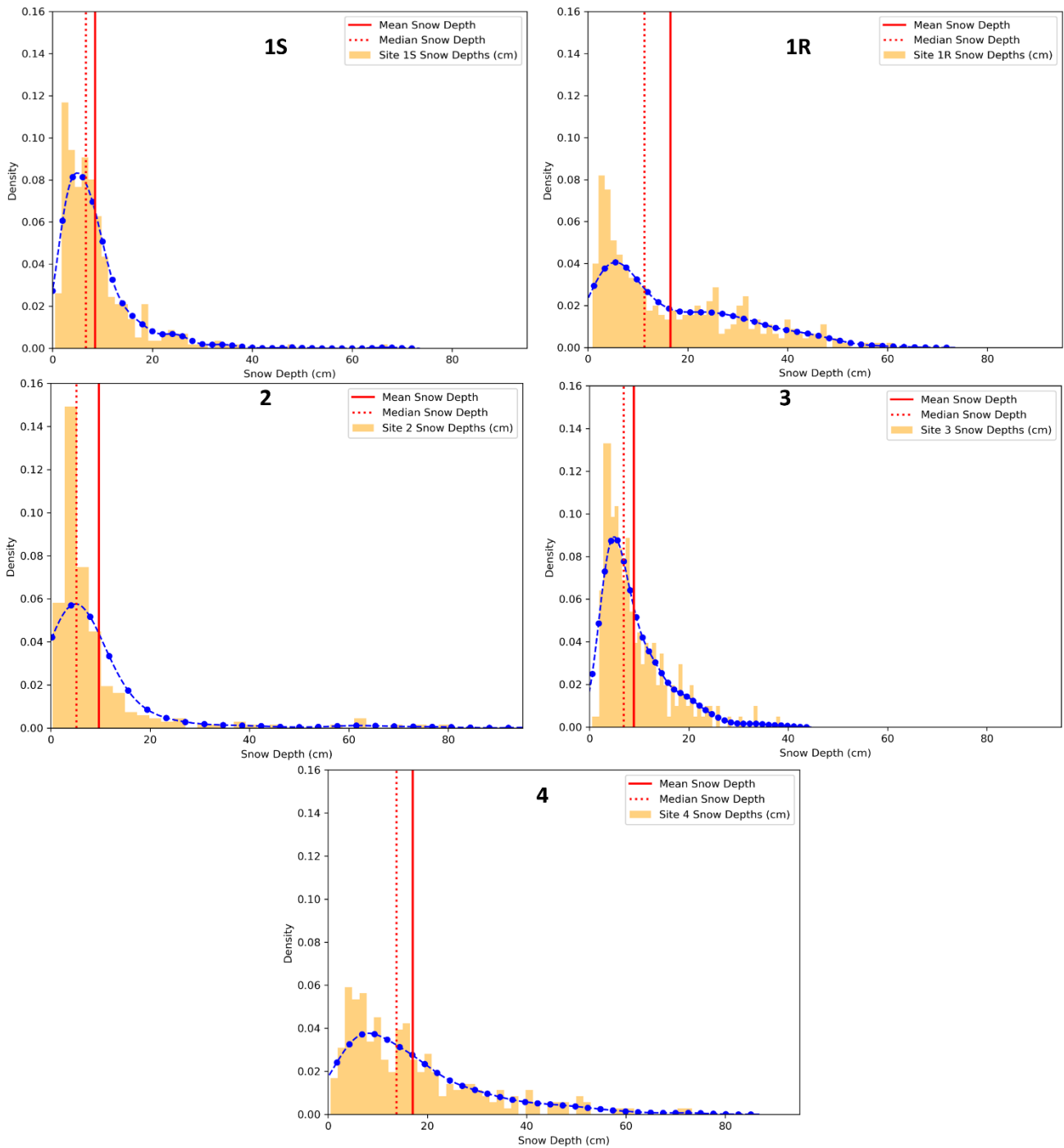
267 Landy et al (2019, 2020) demonstrated the importance of considering surface roughness in the radar data processing. Sea ice
268 surface roughness was computed across the IS2 track using the ATL07 sea ice height product. Surface roughness was
269 calculated as the standard deviation of ATL07 sea ice height product following Farrell et al., (2020). However, instead of the
270 25 km distance set for pan-Arctic studies, the regional differences in surface roughness were calculated over 300-meter length
271 segments to maintain consistency with the spatially averaged ATL07 heights.

272 Previous studies measured or modelled the dominant scattering surface over first-year sea ice (FYI) at Ku-band (Nandan et
273 al., 2017, 2020; Willatt et al., 2011) several to many centimeters above the snow/sea ice interface even for cold snowpacks.
274 Nandan et al. (2017, 2020) argue that when brine is present within the snowpack, the dominant scattering horizon at Ku-band
275 is shifted upwards by approximately 7 cm above the snow/sea ice interface. Mallett et al., (2020) further demonstrated that the
276 use of fixed snow densities introduced significant biases in the snow depth retrievals. Provided snow salinity impacts the
277 location of the Ku-band dominant scattering horizon (Nandan et al., 2017), an assessment was conducted to test the bias
278 introduced by choosing different snow bulk densities by (a) assuming Ku- band microwaves penetrate completely through the
279 snow layers to the sea ice surface and (b) Ku-band microwaves penetrates through layers with snow salinity less than 1 ppt.
280 The corresponding average in-situ snow bulk densities from (a) the complete snow layer (b) snow layers with less than salinity
281 of 1 ppt were used to compute refractive indices followed by respective snow depth calculations. There was negligible
282 difference in the refractive index (<0.05) considering the snow bulk densities with difference in salinity and therefore the
283 average bulk densities from the complete snow pack was used in this study.

284 3. Results

285 3.1 In-Situ Snow Depths and Distributions

286 In-situ snow depths demonstrate significant spatial variability among the four sampled sites (Figure 5). The mean snow depth
287 from the four different sites varies between 9 and 17 cm, and all sites have positively skewed distributions (Figure 5). Site 2
288 also has some exceptionally high snow depths (> 90 cm), corresponding to the ridged areas (Figure 5) and therefore show
289 higher standard deviations (Figure 5). Sites 2 and 3 have similar snow distributions (Figure 5) but the presence of ridging in
290 Site 2 results in a wider tail compared to Site 3. The maximum snow depth of 80 cm was recorded in Site 2 which was picked
291 up directly adjacent to the ridge. Site 4 has the highest mean snow depth (Figure 5) as well as the thickest tailed snow
292 distribution (Figure 5). The distinctive snow depth characteristics were also evident from the standard deviation of snow depth
293 among the four sites. Site 2 which had significant ridging also had the highest standard deviation of snow depth (15.8 cm).
294 Site 1R and Site 4 which had rougher sea ice both had high standard deviations of snow depth (13.7 (Site 1R) and 13.9 (Site
295 4)).



296

297

298

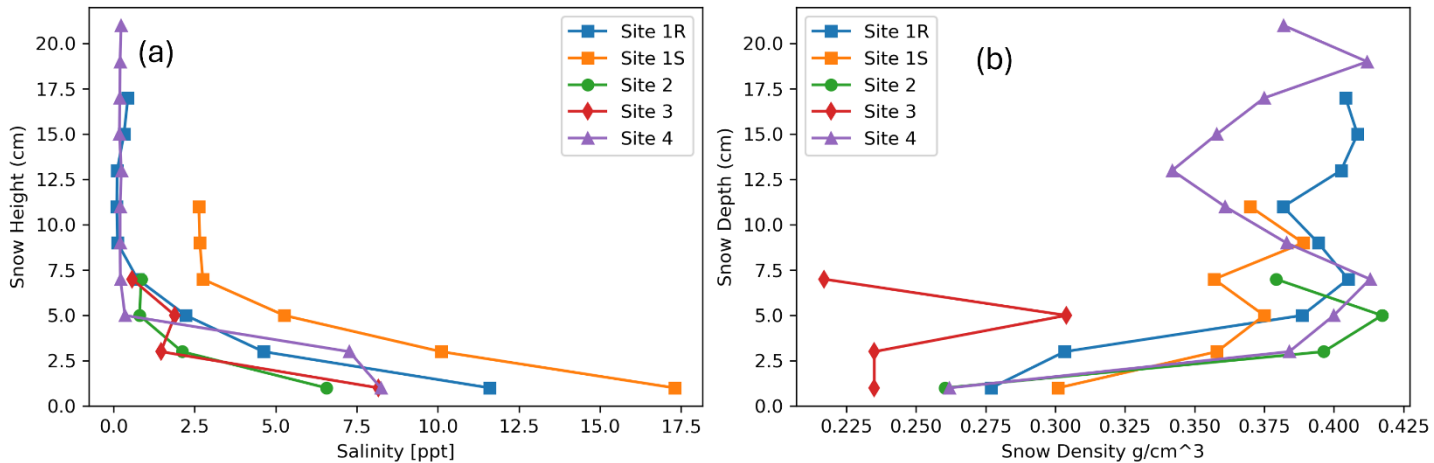
Figure 5 Snow depth distributions from the four in-situ measurement sites along the Cryo2Ice transect. The density distribution curve is shown in blue.

299 **3.2 Snow Geophysical Parameters**

300 Mean snow salinity varies between 1.5 to 3.0 ppt for Sites 1S, 2, 3 and 4, whereas at Site 1S the snow salinity is 6.78 ppt
301 (Figure 6). The mean snow bulk density varies between 0.358 and 0.374 g/cm³ in all sites except Site 3 where the mean snow
302 density is 0.248 g/cm³.

303 Vertical profiles of snow salinity and bulk density present further insights. As shown in Figure 6, the snow density patterns
304 are similar for Sites 1R, 1S, 2 and 4 with bulk density ranging between 0.260 to 0.420 g/cm³ and lower at the base of the
305 snowpack than the surface (Figure 6). The snow density varies in the different snow layers but there is a general trend towards
306 higher densities at 4 to 7 cm above the snow-ice interface at all sites (Figure 6). This is attributed to the presence of a wind
307 slab snow layer most prominent at Sites 1R, 2 and 4.

308 Snow salinity shows higher salinities closer to the snow-ice interface but decreasing with height up the interface (Figure 6 (a)).
309 For snow pits greater than 7.5 cm thick, the salinity is less than 1 ppt closer to the air-snow interface. There is a spike in salinity
310 between 5 to 3 cm from the snow-ice interface at Site 3 that corresponds to the high bulk density snow layer (Figure 6(b)).



311
312 **Figure 6 (a) Snow salinity and (b) Snow density change by snow pack depth at the four snow sampling sites. Zero snow depth in**
313 **both plots represents the snow-ice interface.**

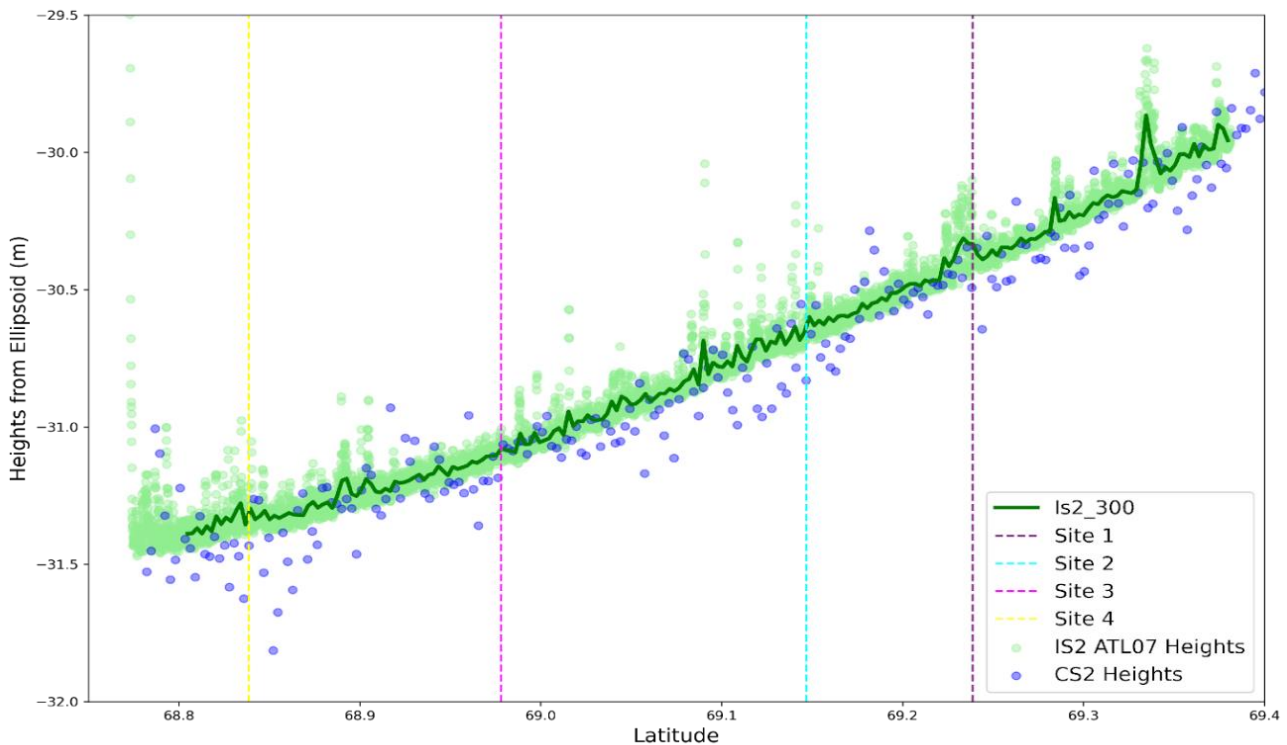
314 **3.3 ICESat-2/Cryosat-2 Derived Snow Depths**

315 Snow depths were calculated based on the ellipsoidal height difference between the IS2 2I and CS2 after adjusting for the
316 difference in tides as explained in Section 2.6 (Figure E1). IS2 2I was closest to the CS2 Points of Closest Approach (POCA)
317 which ensured that the uncertainty due to the difference in spatial collocation of IS2 and CS2 was minimized as explained in
318 Section 2.7. The CS2 ($h(CS2)$) and IS2 ($h(IS2)$) heights show a general pattern of lower CS2 heights relative to co-registered
319 IS2 heights (Figure 7). The correlation of the CS2 ellipsoidal height with the Cryo2Ice snow depth (0.2509) is higher than the
320 IS2 ellipsoidal heights (-0.1213) which implies that the snow depths would be impacted more by the noise in CS2 heights

321 compared to IS2. The $h(IS2)-h(CS2)$ differences range between -26.5 cm and 50.0 cm with a mean difference of 7.9 cm. 20%
322 of the calculated differences are negative which are distributed randomly along the track (Figure 8). While negative snow
323 depths don't have a physical basis, we include them in the subsequent snow depth calculations to not discard the impacts of
324 altimeter noise on the retrieved heights (Fredensborg Hansen et al., 2024). The noises in the CS2 heights as evident in Figure
325 7, corresponds with the large negative snow depth values (Figure 7, Figure 8). Therefore, to reduce the negative bias in snow
326 depths due to the CS2 noise, we exclude negative snow depth values which are two standard deviations away from the mean
327 Cryo2Ice snow depths in the subsequent calculations (Figure 9).

328 The adjusted mean snow depth across the whole Cryo2Ice track is 7.4 cm (Figure 5). A maximum snow depth of 39.4 cm is
329 retrieved from Cryo2Ice, at a length scale of 300 m which is significantly lower than the maximum snow depths measured in
330 situ > 90 cm.

331

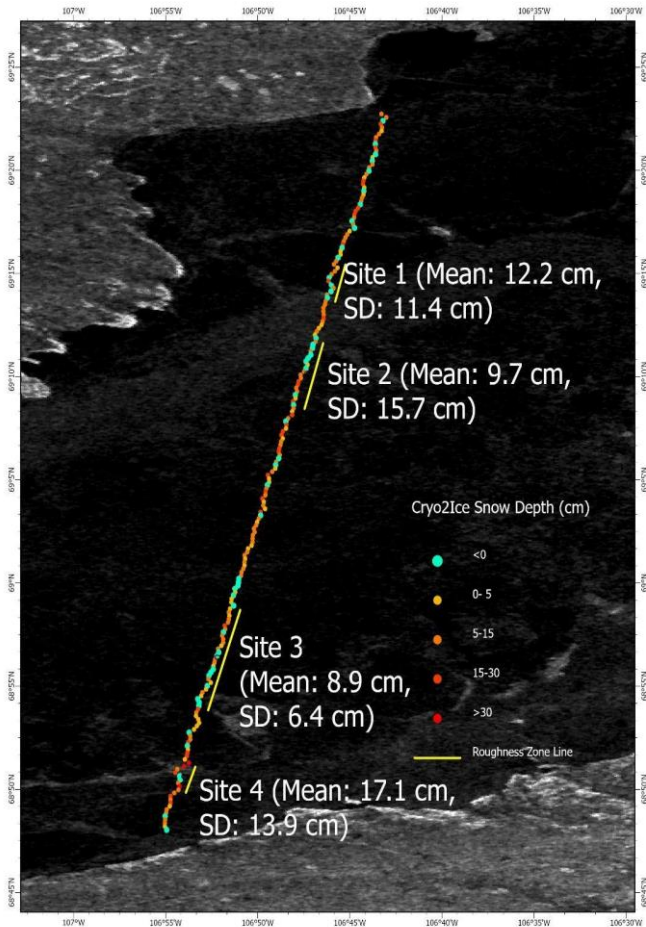


332

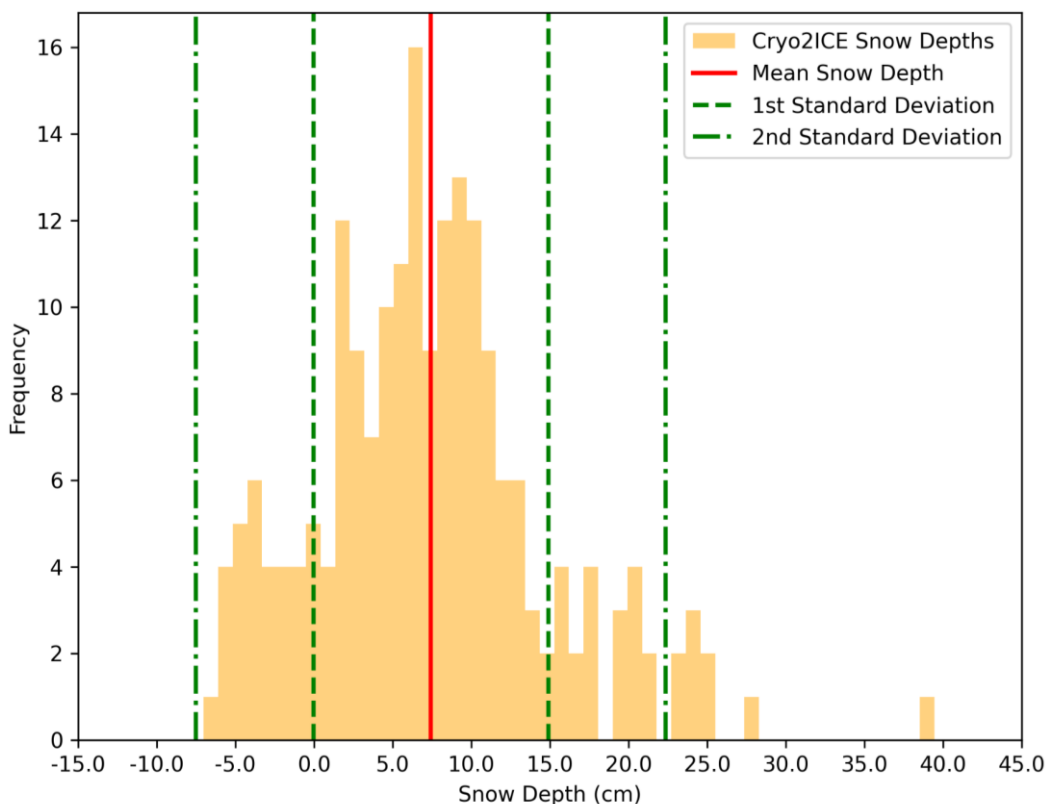
333 **Figure 7 IS2 ATL07 sea ice heights plotted along with CS2 surface heights. Note, the reported heights are relative heights and can**
334 **be negative because of the WGS84 ellipsoid reference heights in the study area. The light green color indicates the raw ATL07**
335 **heights (IS2 ATL07 Heights). The solid green line indicates the aggregated ATL07 heights aggregated every 300 meters (IS2_300).**
336 **The purple color indicates the CS2 Heights.**

337 Snow depths shown in Figure 9 display a right-skewed distribution with a sharper and heavier tail compared to a normal
338 distribution. This is consistent with the distributions obtained from the in-situ snow sites (Figure 5). Analyzing the spatial
339 distribution of the retrieved snow depths demonstrates that there is high spatial variability in the retrieved Cryo2Ice snow

340 depths (Figure 8). The semivariogram analysis indicates that there is spatial autocorrelation among measured snow depths
 341 within 1 km but there is no significant autocorrelation for larger distances, along this specific track. This also implies that
 342 there is significant spatial heterogeneity above the km scale along the 65 km track (Figure 8). The snow depths are correlated
 343 at scales under 1 km which correspond with the lengths of the representative portions of the track delineated with similar
 344 roughness (Figure 8).
 345
 346



347
 348 **Figure 8 Spatial distribution of 300-m scale Cryo2Ice snow depths across the CS2 and IS2 derived track. The background image is**
 349 **a Sentinel-1 HH backscatter image from 5-05-2022. The mean and standard deviation (SD) of the in-situ snow depths are labelled**
 350 **for surveyed sites included inside brackets.**
 351



353

354 **Figure 9** Histogram showing the density distribution of the retrieved snow depth in the native 300 m resolution along the Cryo2Ice
 355 track with the mean and the median snow depths. Negative snow depths greater than 2 standard deviations from the mean snow
 356 depth were removed to reduce the impact of CS2 noise.

357 4 Discussion

358 4.1 Snow Depth: Cryo2Ice vs In-situ

359 Previous field observations from Yackel et al. (2019) and Nandan et al. (2020) suggest that mean snow depth on FYI in Dease
 360 Strait during late winter ranges between 10 and 30 cm depth (Table 1). While our mean in-stu snow depth measurements (11.9
 361 cm) within the typical range reported in previous surveys, we see that the Cryo2Ice mean snow depth (7.44 cm) underestimated
 362 the observed snow depths (Table 1).

363 **Table 1 In-situ snow depth measurements at Dease Strait. The range of mean snow depths represents the range of mean snow depths**
 364 **retrieved from the sampled sites.**

365

Sampling Period	Mean Snow Depth (cm)	Number of Sites Sampled	Total Number of Samples	Sampling Technique	Reference
20 April to 9 June, 2014	13.5	24	24	Snow Pits	Campbell et al., (2016)
12 May to 17 June, 2014	20.8	2	60	Meter Rule Sampling	Diaz et al., (2014)
19-22 April, 2014	12.0/18.0	20	5200	Meter Rule Sampling	Zheng et al., (2017)
23-26 May, 2016	12.0/22.0	4	2100	Meter Rule Sampling	Moon et al., (2019)
01-08 April, 2017	17.0/ 35.0	5	2161	Magnaprobe Sampling	Moon et al., (2019)
17-19 May, 2018	20.9 / 21.8	3		Magnaprobe Sampling	Yackel et al., (2019)
1 May, 2022	11.9	4	1596	Magnaprobe Sampling	This Study
Cryo2Ice Snow Depths	7.44 (Mean), 39.4(Maximum)				

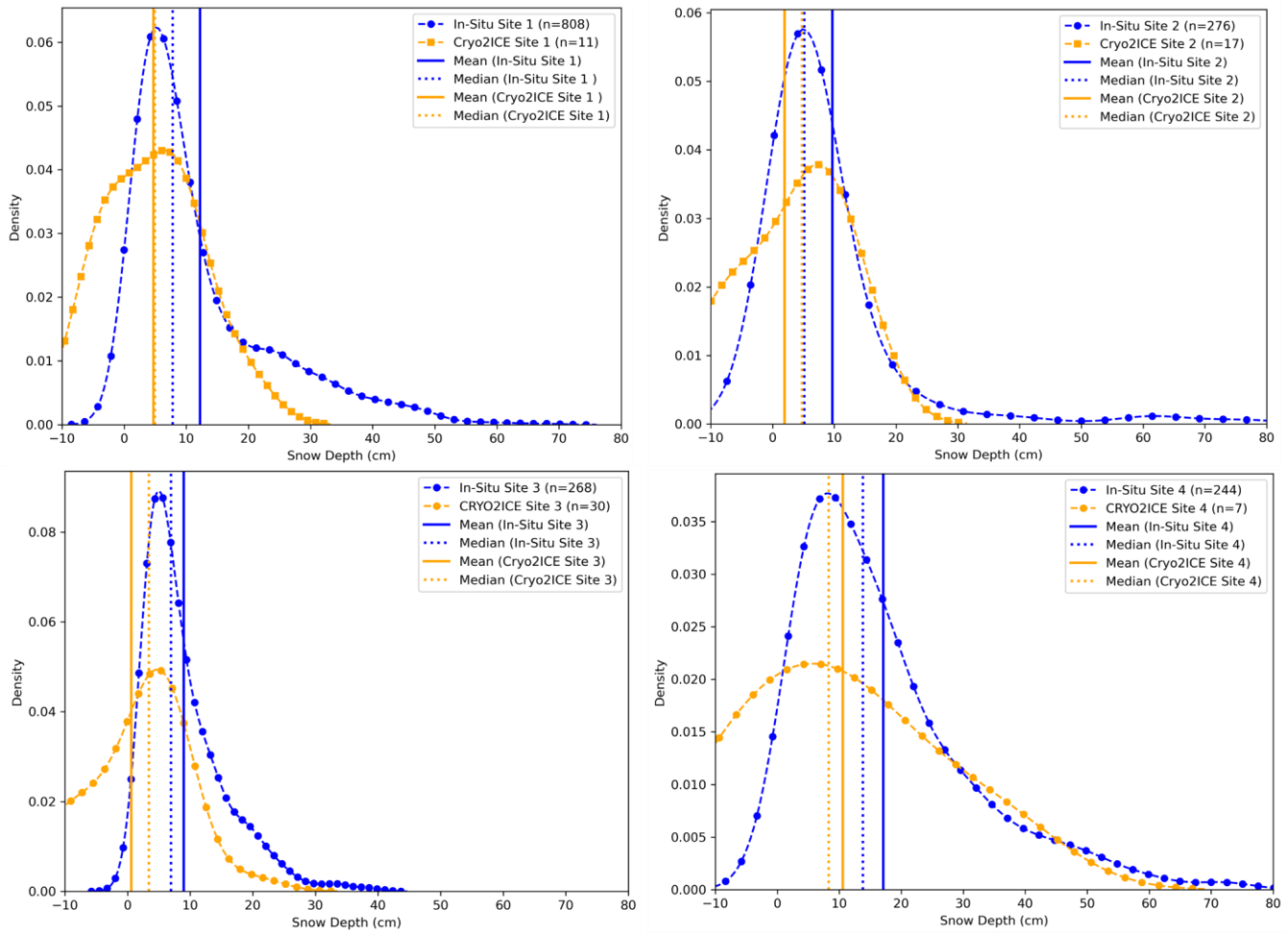
366

367 Cryo2Ice snow depths showed similar relative patterns when compared to in-situ snow depth sampling. The thinnest (Site 3)
 368 and thickest (Site 4) mean snow depths found in the in-situ measurements are corroborated with Cryo2Ice snow depths as well.
 369 The Kruskal-Wallis non-parametric test was conducted to assess statistically significant differences between the snow depths
 370 retrieved from the in-situ and Cryo2Ice. The test results show significant difference between in-situ sites which was also
 371 evident in the corresponding Cryo2Ice snow depths.

372 Considering the median bias of snow depths reduces the impact of the outliers i.e. the retrieved negative snow depths as well,
373 Cryo2Ice snow depths are on average 3.07 cm thinner than the in-situ data, which is a 1 cm larger difference than the manual
374 tidal correction we applied to compare the CS2 and IS2 track heights (i.e., the largest known systematic uncertainty during
375 processing) (Figure F1). This pattern of a few cm mean snow depth underestimations by Cryo2Ice is consistently observed
376 across four sites (Figure 10)(Table F1). It is evident that while IS2 has a much finer resolution, the larger footprint of CS2
377 means that the spatial variability of snow depths under the kilometer scale are not well represented by Cryo2Ice. For instance,
378 the Cryo2Ice snow depths are consistently truncated at the thick end of the distribution, with at least some portion of the in-
379 situ distributions above ~30-50 cm seemingly unresolved from space (Figure 10).

380 We also notice that the Cryo2Ice snow depth distributions are generally wider than the in-situ distributions which is due to the
381 impact of the significant negative snow depths which are included in the calculation. These negative snow depths, while
382 included in the initial calculations to reflect the true native resolution results, don't have a physical basis, leading to artificial
383 widening of the distributions in Figure 10.

384



385

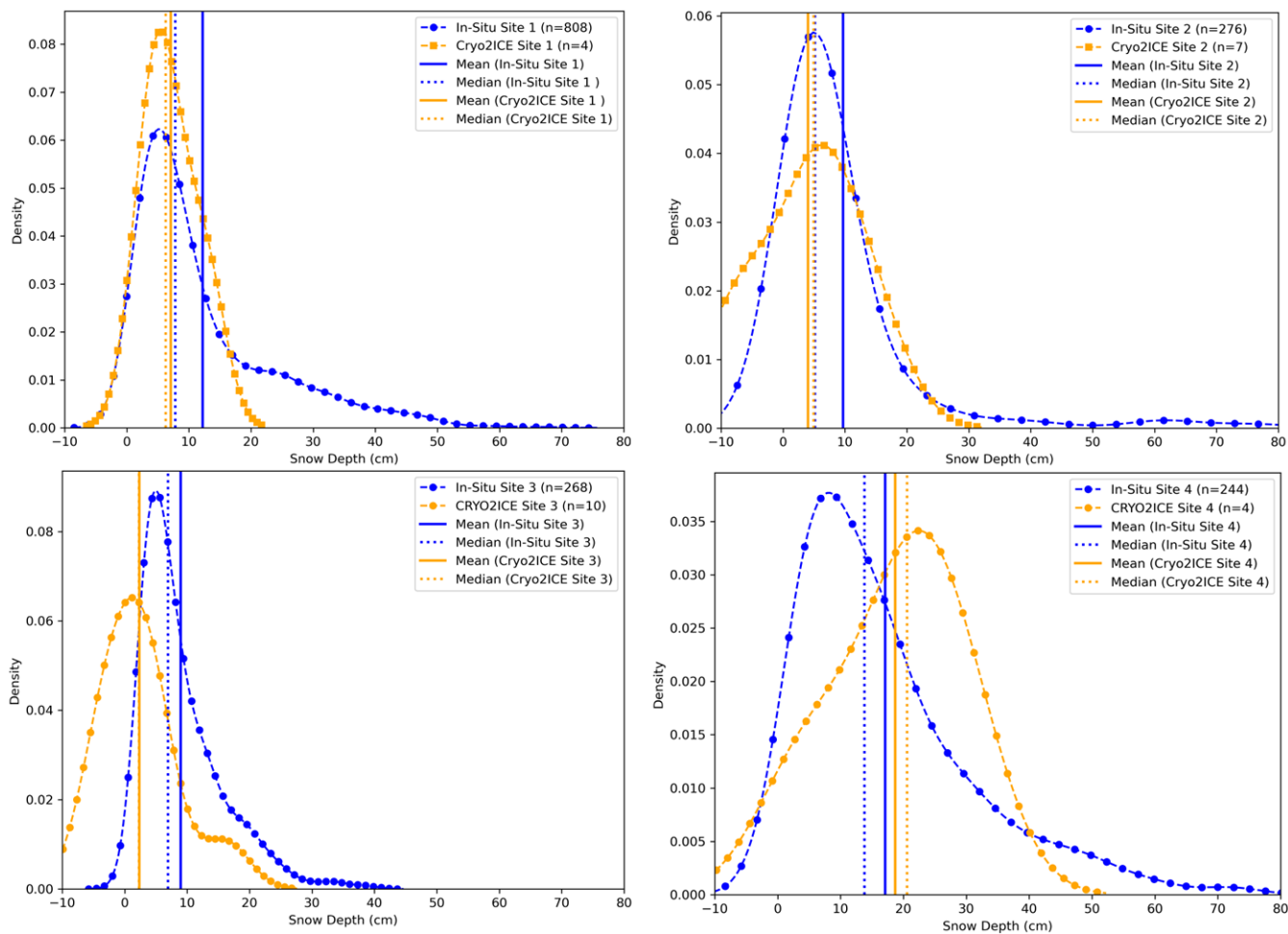
386 **Figure 10** Probability Density plots comparing In-Situ snow depths to Cryo2Ice retrieved snow depths along with the median and
 387 mean values. Different snow bulk densities were used to calculate the refractive index and subsequently Cryo2Ice snow depths for
 388 each site (Site 1-0.399 g/cm³, Site 2- 0.398 g/cm³, Site 3- 0.217 g/cm³, Site 4-0.381 g/cm³). The detailed statistics for the
 389 comparison are provided in Table F1.

390 **4.2 Adjusting for the Difference in CS2 and IS2 Footprint**

391 As noted in Section 4.2, the difference in CS2 and IS2 footprint size with IS2 having a significantly smaller footprint compared
 392 to CS2 leads to a significant underestimation of the retrieved snow depths in the native 300 m resolution. Therefore, to reduce
 393 the impact of this artificial underestimation of the distribution, we average both IS2 and CS2 over a larger along-track distance.
 394 While averaging the CS2 and IS2 over 1-km causes some of the prominent roughness features such as ridges to be missed by
 395 Cryo2Ice, the snow depths from the 1-km CS2 and IS2 averaged heights are more realistic representations of the snow
 396 distributions when compared to in-situ (Figure 11). The average snow depth from the 1-km averaged CS2 and IS2 heights
 397 represents the overall shapes of the in-situ snow depths better compared to the native 300-meter averaged heights (Figure 11).
 398 The shapes of the distributions are well represented especially in Site 1 and 2. We also notice that shapes of the Cryo2Ice snow
 399 depth distributions match best in Site 1 and 2 compared to in-situ. However, the general underestimation of snow depths is
 400 reflected within most of the Sites (Site 1, 2, 3) except Site 4 which seems to overestimate the snow depth (Figure F2). The
 401 average snow depth retrieved from the 1-km averaged product is 7.80 cm which is slightly higher than the 300-meter averaged

402 product presented in Section 3.3. The median bias between the in-situ and the 1 km averaged product is less than 2 cm in Sites
403 1 and 2. (Figure 11) (Tabel F2).

404 Comparing the shapes of the distributions, we see that almost all the sites have similar snow depth distributions compared to
405 in-situ sites (Figure 11). However, a significant portion of the tails of the distributions are still missing which was also evident
406 in the 300 m snow depth product. While the shapes of the distributions in Sites 3 and 4 are similar compared to in-situ, the
407 peaks of the distribution don't coincide well. Cryo2Ice snow depths in Site 1 has the most similar distribution to in-situ
408 compared to the other sites. In Site 2 we also see very similar snow depth distributions between Cryo2Ice and in-situ even
409 between the 20 to 30 cm snow depths. While the shapes of the distributions match well in Site 3, we see a shift towards negative
410 snow depths indicating that negative snow depths caused by noise in CS2 have larger impacts here in the smoother sea ice.
411 Cryo2Ice seems to perform worst in Site 4 which is the roughest sea ice zone, with Cryo2Ice snow depths being overestimated
412 when compared to in-situ. This is also evident in the shapes of the 1-km adjusted snow depth product which seems to be
413 skewed towards higher snow depth values (Figure 11). Therefore, after adjusting for the difference in footprint size and
414 averaging over 1-km along-track distance, the overall snow depth distributions are more similar to in-situ for the majority of
415 the sites.



416

417 **Figure 11 Probability Density plots comparing In-Situ snow depths to Cryo2Ice retrieved snow depths retrieved from 1-km averaged**
418 **CS2 and IS2 heights along with the median and mean snow depth values. Different snow bulk densities were used to calculate the**

419 refractive index and subsequently Cryo2Ice snow depths for each site (Site 1-0.399 g/cm³, Site 2- 0.398 g/cm³, Site 3- 0.217
420 g/cm³, Site 4-0.381 g/cm³). The detailed statistics for the comparison are provided in Table F2

421 422 **4.3 Snow Geophysical Properties and Cryo2Ice Retrievals**

423 Both snow salinity and bulk density changes across the snowpack layer impacts the IS2 laser and CS2 radar waveform
424 interactions with the snowpack. While the IS2 green laser is mostly impacted by the air-snow interface conditions, CS2 radar
425 waveforms interact with different layers of the snowpack and the dominant scattering horizon and subsequently radar heights
426 are impacted by the snow properties. There were significant differences among the snow salinity and density characteristics
427 (Figure 6) between the surveyed sites. However, we notice that higher snow depths i.e. greater than 30 cm were picked up
428 better in Site 4 which also had the lowest mean salinity with 17 cm out of the 22 cm deep snowpack being non-saline. Therefore,
429 the maximum intensity of the CS2 backscatter may have been sourced from closer to the sea-ice interface in Site 4. On the
430 contrary, highly saline layers can potentially raise the height of dominant scattering intensity of the Ku-band radar leading to
431 overestimated CS2 heights ($h(CS2)$) and subsequently lower mean snow depth compared to in-situ values. This phenomenon
432 of snow depth underestimation was evident in Sites 1 and 2 potentially because of the sharp increase in snow salinity within
433 the first 5 cm (from the air-snow interface) of the snowpack (Figure 6) and may have contributed to ~ 2 cm underestimation
434 of Cryo2Ice snow depths.

435 The impact of snow bulk density on the Cryo2Ice retrievals was less likely except for the presence of wind-slab layers which
436 are identified as stark increases in snow bulk densities within the snowpack. The wind-slab layers were identified in Site 1R
437 where the density reached to 0.425 g/cm³ compared to 0.358 to 0.374 g/cm³ on average throughout the snowpack which may
438 have caused hindrance to Ku-band penetration which may have contributed to median underestimations. The presence of this
439 high-density snow layer along with the reduction in Ku-band speed due to power attenuation of Ku-band microwaves may
440 potentially cause a cumulative upward shift of the dominant scattering horizon resulting in underestimation of snow depths.
441 However, it is difficult to ascertain such uncertainties to a single physical factor due to interdependency of the processes.

442 **4.4 Sea Surface Height Estimation and Cryo2Ice Retrievals**

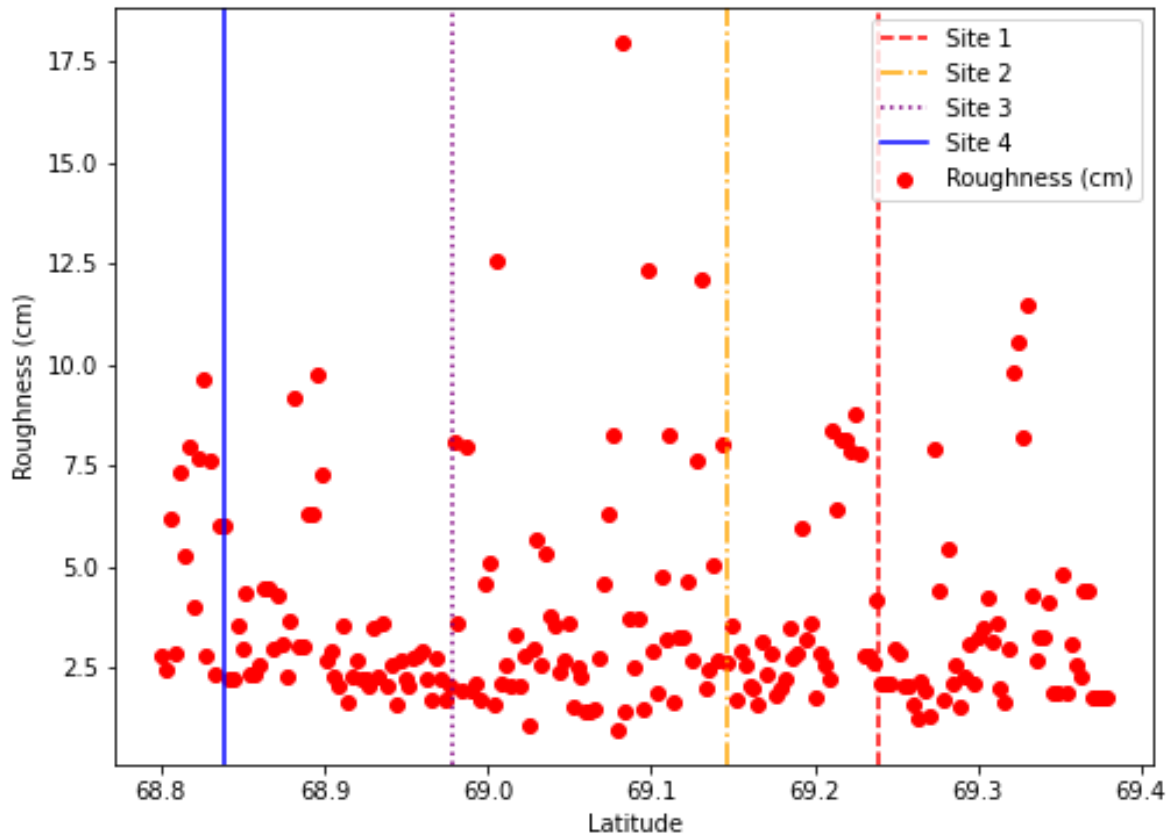
443 Canadian Hydrographic Service (CHS) tidal predictions for 29 April 2022 suggest the satellite overpasses occurred during a
444 low tide period. According to the predictions, the water level was 6 cm higher for the IS2 pass at 21:18 UTC than for the CS2
445 pass at 22:35 UTC (Figure C1). This 6 cm water level difference should ideally be accounted for by the difference in IS2 and
446 CS2 ocean tide corrections. The IS2 ATL07 heights were reduced by a mean ocean tide correction of -0.71 cm whereas the
447 CS2 Heights reduced by an average ocean tide correction of -8.64 cm. Therefore, the difference between IS2 heights and CS2
448 heights was increased by 7.9 cm due to the ocean tide correction adjustment but the CHS predictions suggest it should have
449 been only 6.0 cm. This 1.9 cm difference would introduce a 25.5 % bias in retrieved snow depths, given the approx. mean
450 snow depths we measured in-situ. This error could be attributed to the ocean tide corrections used in IS2 and CS2 originating

451 from two different models i.e. GOT 4.8 (IS2) and FES 2004 (CS2). To put this source of error into wider context, past CS2
452 and IS2 coincident tracks from 15-04-2021 and 14-05-2021 were also analysed. We found a bias of 2 to 5 cm when compared
453 with the CHS dataset, meaning that we can expect ~15-40% systematic uncertainty in Cryo2Ice retrieved snow depths owing
454 to the uncertainty in tidal differences between satellite passes. This is a significant uncertainty, but it is systematic and varies
455 at the length-scale of the tidal corrections (100s km), so it will not affect the *relative* variations in retrieved snow depth along
456 track, only their *absolute* magnitude. Therefore, Cryo2Ice seems capable of measuring the relative variations in snow depth
457 between different locations of the CAA without the availability of sea surface reference tie-points.

458 **4.5 Surface Roughness and Cryo2Ice retrievals**

459 Surface roughness calculated from IS2 was used to analyze the Cryo2Ice snow depths between sites with different roughness.
460 There was only a weak positive correlation (R^2 0.04) between surface roughness retrieved from IS2 and Cryo2Ice snow depths.
461 Site 4 had the highest mean surface roughness (4.58 cm) whereas the other sites had roughness ranging between 2.4-2.7 cm.
462 Although there was significant ridging in Site 2 and IS2 does pick up some of the ridges (Figure 7), the mean surface roughness
463 is low (2.48 cm) because of the extensive areas of thin snow cover which dominates the laser returns. Site 4 had the highest
464 snow depth as well as highest surface roughness from IS2 which also corresponds with the highest median bias (Table F2).
465 [Significant variation in surface type in Site 4 is also evident from the large variation retrieved backscatter from Sentinel-1 \(-](#)
466 [5dB to 3dB\)\(Figure 4\(b\)\) which was not very well represented from the snow depth estimations from Cryo2Ice.](#) Therefore, we
467 notice that Cryo2Ice performs poorly in regions with relatively high surface roughness. The presence of isolated ridges and
468 the deeper snow accumulated around them may have been missed by the CryoSat-2 radar given the larger impact of level ice
469 versus ridges on the backscattered power which may explain the underestimation in Sites 1 and 2. The ridge heights may also
470 be underestimated with current ICESat-2 processing methods (Ricker et al., 2023) meaning that snow depths would be
471 underestimated. The surface roughness from IS2 computed and compared well to the roughness features picked up from the
472 snow depth variations with higher roughness zones having higher snow depths from Cryo2Ice e.g. Site 4. However, the
473 difference in spatial resolutions between IS2 and snow depths from Cryo2Ice means that finer scale surface roughness features
474 were missed by Cryo2Ice especially in the 1-km averaged snow depth product.

475



476

477 **Figure 12** Variation in surface roughness along the Cryo2Ice track at the four in-situ snow thickness validation sites

478

479 **5 Conclusion**

480 Accurate snow depth monitoring over landfast ice in the Canadian Arctic Archipelago (CAA) is important for communities
 481 that rely on landfast ice for transportation and their livelihood (Mahoney et al., 2009). It is imperative to monitor snow depth
 482 in the CAA as there have been reports of declining snow depths at a rate of 0.8 cm per decade in Cambridge Bay and at other
 483 locations in the CAA (Howell et al., 2016; Lam et al., 2023). Moreover, the reported snow depth on sea ice trends were highly
 484 correlated to the declining sea ice thickness. Therefore, this study explores the potential of retrieving snow depth using
 485 Cryo2Ice in a lead-less regions of the Canadian Arctic Archipelago. ~~While Freesborgen Hansen et al (2024) have compared
 486 snow depths over larger segments (7 km) and used snow depth products from passive microwave, snow models or
 487 climatologies, this study is the first comparison of Cryo2ice snow depths to in situ snow depth retrievals over 300 meter and
 488 1 kilo meter segments.~~ Snow depth from Cryo2Ice is retrieved based on the elevation difference between IS2 and CS2 sea ice
 489 heights from a common ellipsoid as opposed to the popular freeboard differencing method. The instantaneous difference in

490 sea level between the ~~77-minute~~77-minute difference between the CS2 and IS2 passes is accounted for by adjusting the ocean
491 tide corrections with local tide model predictions. The snow depths retrieved from Cryo2Ice compare favourably with in-situ
492 snow depth measurements when averaged over 1-km segments of the tracks. The relative snow depth patterns from in-situ
493 field sites were corroborated with Cryo2Ice measurements, i.e. the thinnest and thickest snow depth regions were picked up
494 correctly by Cryo2Ice. The 300 meter averaged Cryo2Ice snow depths shows an average of 7.44 cm which is slightly
495 underestimated when compared to in-situ measurements from this study (11.9 cm) and previous studies conducted at the Dease
496 Strait. While the ~2 to 3 cm underestimation demonstrates that Cryo2Ice can estimate snow depth with reasonable accuracy
497 after adjusting for the tidal uncertainty (Fredensborgsborger Hansen et al., (2024) reports uncertainties of 10-11 cm
498 uncertainties), there are still significant sources of both systematic and random uncertainties that need to be addressed. We
499 note that median biases ranging from 2 to 5.5 cm are reported among the different Sites which is often higher than the tidal
500 correction applied (1.9 cm).

501 The site-wise comparison between in-situ snow depths and Cryo2Ice snow depths show that Cryo2Ice performs well in regions
502 with moderately thin and smooth snow on sea ice i.e. ranging between 5 to 20 cm while it struggles to pick up snow depths
503 greater than 30 cm irrespective of the roughness characteristics. This phenomenon is largely attributed to the difference in
504 footprint size between CS2 and IS2 where the large footprint of CS2 missed a lot of the high snow depth sites particularly the
505 ones close to the ridges which are otherwise picked up by IS2. We also notice that negative snow depths mostly retrieved from
506 rougher sea ice zones spatially coincides with the noisy CS2 heights which are significantly higher than the IS2 heights. These
507 negative snow depths (20 % of the Cryo2Ice estimates) significantly skew the snow depth distributions retrieved. We note that
508 the number of negative freeboards (20%) is much larger than the 3% negative snow depths reported in Fredensborg Hansen et
509 al., (2024) which we believe is mostly due to the fact that this study considers a single track averaging averaging over a 300
510 m and 1-km window compared to a 7-km window in the aforementioned study. Therefore, we see that the noisy nature of CS2
511 data especially in landfast ice plays a major factor in the underestimation of the snow depths retrieved from Cryo2Ice.
512 Differences in the shapes of the distributions from in-situ sites and representative roughness zones of the Cryo2Ice are mostly
513 a result of the difference in sampling resolutions of Cryo2Ice (~300 m) and the in-situ measurements (5 m). The tails of the
514 in-situ snow depth distributions (> 40 cm) were largely missed by Cryo2Ice and the Cryo2Ice snow depth retrieval accuracy
515 is impacted by the presence of sea ice ridges. This impact leads to an artificial widening of the snow depth distributions which
516 are obtained in the native 300-meter resolution. After adjusting for this difference by averaging both IS2 and CS2 heights over
517 1-km instead, more realistic snow depth distributions are obtained. We note that while Cryo2Ice generally underestimates
518 snow depths by 2 to 4 cm compared to in-situ, the 1-km averaged snow depths also show the possibility of overestimation over
519 significantly rough ice. Therefore, future studies should consider analyzing both the 300 meter resolution product and the 1-
520 km averaged product in order to get both the meter scale snow depth variations from the 300 meter snow depths as well as the
521 more representative snow depth distribution from the 1-km averaged snow depths.

522 Snow geophysical properties, especially snow salinity in the deepest few centimeters of the snowpack, may impact the
523 dominant scattering surface of the CS2 radar, resulting in the scattering surface shifted upwards into the snowpack, leading

524 ~~being further above the snow-ice interface which return and can leads~~ to underestimation of the snow depths. The 1-km
525 averaged snow depth was slightly underestimated three out of four sites compared to in-situ measurements; however the
526 median biases compared to in-situ are less than 5 cm. This study identifies several different sources of uncertainty such as
527 noise in the CS2 heights, surface roughness and snow geophysical properties which significantly impact the snow depth
528 retrievals in addition to the uncertainty due to the tidal correction. However, it is difficult to determine given the few
529 centimeters of bias to snow geophysical process, surface roughness and/or errors in the altimeters' tidal corrections given that
530 a lot of these uncertainties are inter-related and are highly variable among different length scales. Therefore, a further
531 comprehensive study across different regions is required to isolate the impacts of these uncertainties and determine their
532 contributions to the total uncertainty. Additionally, there are uncertainties such as the use of a fixed threshold retracker in CS2
533 which is not tuned for the landfast sea ice and uncertainties associated with the IS2 fine-tracker that may also contribute
534 significantly to the snow depth retrievals. Therefore, further studies are required in different lead-less regions under varying
535 snow conditions for improved insights into the sources of bias in snow depth retrievals from Cryo2Ice. It is also noteworthy
536 that the suggested method of using ellipsoidal heights from IS2 and CS2 with the tidal correction may also be applied in regions
537 beyond the landfast sea ice in the Canadian Arctic Archipelago (CAA). However, as the current method relies on using tidal
538 gauge station data from a nearby station, this method may not be directly applicable for regions that don't have a tidal gauge
539 station nearby. However, tidal predictions from tide models that consider the impact of sea ice on the tidal amplitude such as
540 Nucleus for European Modelling of the Ocean (NEMO) may be used instead to estimate the difference in tides between the
541 passes. While this study suggests the use of Ellipsoidal heights for landfast ice, the freeboard differencing approach as
542 suggested in Kwok et al., (2020) is better suited for regions where getting a direct estimation of the sea surface height and
543 direct estimates of the freeboard are available. Findings from this study are encouraging for estimating snow depth on land-
544 fast sea ice in lead-less regions using Cryo2Ice and for future coincident laser-radar or dual-frequency altimeter missions.

545 **Data Availability**

546 ICESat-2 ATL07 data may be accessed from the NSIDC website (See: <https://nsidc.org/data/atl07ql/versions/6#anchor-2>).
547 Cryosat-2 data may be accessed from ESA (<https://eocat.esa.int/>). The snow depth validation dataset is available from the
548 CanWin Data Hub https://canwin-datahub.ad.umanitoba.ca/data/dataset/cambridge_bay_snowdepth_apr2022.

550 **Author Contribution**

551 MS, JS and DI were involved in the conceptualization of the study. MS, JS, JY, HML and VN were involved in planning of
552 the field campaign. JS acquired the funding for the research. MS, JY and HML collected the snow and sea ice physical property
553 validation data from the field. MS, JS, DI, JL and VN were involved in formulating the methodology for the analysis. MS
554 prepared the original draft. All co-authors were involved in the review and editing process.

555 **Competing Interests**

556 At least one of the (co-)authors is a member of the editorial board of The Cryosphere.

557 **Acknowledgements**

558 The authors would like to acknowledge Torsten Geldsetzer from the University of Calgary for his input during the planning
559 stages of the Cambridge Bay campaign. We acknowledge Dr. Nathan Kurtz from NASA for providing early ICESat-2 ATL07
560 release 006 data which was vital for the analysis. MS was supported by ArcticNet (Grant Number #52551), Julienne Stroeve's
561 NSERC Canada 150 Chair (Grant Number #50297) and NASA Award 80NSSC20K1121, John Yackel's NSERC Discovery
562 Grant (RGPIN-2017-04888) and University of Manitoba Graduate Student Fellowship (UMGF). We also acknowledge support
563 from ArcticNet Field Aircraft Support for the helicopter support.
564

565 **References**

566 Andersen, O. B., Nilsen, K., Sørensen, L. S., Skourup, H., Andersen, N. H., Nagler, T., Wuite, J., Kouraev, A., Zakharova, E.,
567 and Fernandez, D.: Arctic freshwater fluxes from earth observation data: International Review Workshop on Satellite Altimetry
568 Cal/Val Activities and Applications, Fiducial Reference Measurements for Altimetry, 97–103,
569 https://doi.org/10.1007/1345_2019_75, 2019.

570 Andreas, E. L., Jordan, R. E., and Makshtas, A. P.: Parameterizing turbulent exchange over sea ice: the ice station weddell
571 results, *Boundary-Layer Meteorology*, 114, 439–460, <https://doi.org/10.1007/s10546-004-1414-7>, 2005.

572 Bagnardi, M., Kurtz, N. T., Petty, A. A., and Kwok, R.: Sea Surface Height Anomalies of the Arctic Ocean From ICESat-2:
573 A First Examination and Comparisons With CryoSat-2, *Geophys. Res. Lett.*, 48, e2021GL093155,
574 <https://doi.org/10.1029/2021GL093155>, 2021.

575 Beaven, S. G., Lockhart, G. L., Gogineni, S. P., Hossetnmostafa, A. R., Jezek, K., Gow, A. J., Perovich, D. K., Fung, A. K.,
576 And Tjuatja, S.: Laboratory measurements of radar backscatter from bare and snow-covered saline ice sheets, *International*
577 *Journal of Remote Sensing*, 16, 851–876, <https://doi.org/10.1080/01431169508954448>, 1995.

578 Blanchard-Wrigglesworth, E., Webster, M. A., Farrell, S. L., and Bitz, C. M.: Reconstruction of Snow on Arctic Sea Ice,
579 *Journal of Geophysical Research: Oceans*, 123, 3588–3602, <https://doi.org/10.1002/2017JC013364>, 2018.

580 Brunt, K. M., Neumann, T. A., and Smith, B. E.: Assessment of ICESat-2 Ice Sheet Surface Heights, Based on Comparisons
581 Over the Interior of the Antarctic Ice Sheet, *Geophysical Research Letters*, 46, 13072–13078,
582 <https://doi.org/10.1029/2019GL084886>, 2019.

583 Cafarella, S. M., Scharien, R., Geldsetzer, T., Howell, S., Haas, C., Segal, R., and Nasonova, S.: Estimation of Level and
584 Deformed First-Year Sea Ice Surface Roughness in the Canadian Arctic Archipelago from C- and L-Band Synthetic Aperture
585 Radar, *Can. J. Remote Sens.*, 45, 457–475, <https://doi.org/10.1080/07038992.2019.1647102>, 2019.

586 Campbell, K., Mundy, C. J., Landy, J. C., Delaforge, A., Michel, C., and Rysgaard, S.: Community dynamics of bottom-ice
587 algae in Dease Strait of the Canadian Arctic, *Prog. Oceanogr.*, 149, 27–39, <https://doi.org/10.1016/j.pocean.2016.10.005>, 2016.

588 De Rijke-Thomas, C., Landy, J. C., Mallett, R., Willatt, R. C., Tsamados, M., and King, J.: Airborne Investigation of Quasi-
589 Specular Ku-Band Radar Scattering for Satellite Altimetry Over Snow-Covered Arctic Sea Ice, *IEEE Trans. Geosci. Remote
590 Sens.*, 61, 1–19, <https://doi.org/10.1109/TGRS.2023.3318263>, 2023.

591 Diaz, A., Ehn, J. K., Landy, J. C., Else, B. G. T., Campbell, K., and Papakyriakou, T. N.: The Energetics of Extensive Meltwater
592 Flooding of Level Arctic Sea Ice, *J. Geophys. Res. Oceans*, 123, 8730–8748, <https://doi.org/10.1029/2018JC014045>, 2018.

593 Eicken, H., Grenfell, T. C., Perovich, D. K., Richter-Menge, J. A., and Frey, K.: Hydraulic controls of summer Arctic pack ice
594 albedo, *Journal of Geophysical Research: Oceans*, 109, <https://doi.org/10.1029/2003JC001989>, 2004.

595 ESA: CryoSat-2 Product Handbook, 2013.

596 ESA: About CRYO2ICE - Earth Online:<https://earth.esa.int/eogateway/missions/cryosat/Cryo2Ice>, last access: 20 October
597 2023, 2020.

598 Farrell, S., Duncan, K., Yi, D., Hendricks, S., Ricker, R., Buckley, E., and Baney, O.: Optimizing Dual-Band Satellite
599 Altimetry to Map Declining Arctic Sea Ice, 2021, C31B-05, 2021.

600 Fons, S. W., Kurtz, N. T., Bagnardi, M., Petty, A. A., and Tilling, R. L.: Assessing CryoSat-2 Antarctic Snow Freeboard
601 Retrievals Using Data From ICESat-2, *Earth Space Sci.*, 8, e2021EA001728, <https://doi.org/10.1029/2021EA001728>, 2021.

602 Fredensborg Hansen, R. M., Skourup, H., Rinne, E., Høyland, K. V., Landy, J. C., Merkouriadi, I., and Forsberg, R.: Arctic
603 Freeboard and Snow Depth From Near-Coincident CryoSat-2 and ICESat-2 (CRYO2ICE) Observations: A First Examination
604 of Winter Sea Ice During 2020–2022, *Earth Space Sci.*, 11, e2023EA003313, <https://doi.org/10.1029/2023EA003313>, 2024.

605 Galley, R. J., Else, B. G. T., Howell, S. E. L., Lukovich, J. V., And Barber, D. G.: Landfast Sea Ice Conditions in the Canadian
606 Arctic: 1983-2009, *Arctic*, 65, 133–144, 2012.

607 Howell, S. E. L., Laliberté, F., Kwok, R., Derksen, C., and King, J.: Landfast ice thickness in the Canadian Arctic Archipelago
608 from observations and models, *The Cryosphere*, 10, 1463–1475, <https://doi.org/10.5194/tc-10-1463-2016>, 2016.

609 Kacimi, S. and Kwok, R.: The Antarctic sea ice cover from ICESat-2 and CryoSat-2: freeboard, snow depth, and ice thickness,
610 *The Cryosphere*, 14, 4453–4474, <https://doi.org/10.5194/tc-14-4453-2020>, 2020.

611 Kern, S., Khvorostovsky, K., Skourup, H., Rinne, E., Parsakhoo, Z. S., Djepa, V., Wadhams, P., and Sandven, S.: The impact
612 of snow depth, snow density and ice density on sea ice thickness retrieval from satellite radar altimetry: results from the ESA-
613 CCI Sea Ice ECV Project Round Robin Exercise, *The Cryosphere*, 9, 37–52, <https://doi.org/10.5194/tc-9-37-2015>, 2015.

614 Kurtz, N. T. and Farrell, S. L.: Large-scale surveys of snow depth on Arctic sea ice from Operation IceBridge, *Geophysical
615 Research Letters*, 38, <https://doi.org/10.1029/2011GL049216>, 2011.

616 Kwok, R. and Markus, T.: Potential basin-scale estimates of Arctic snow depth with sea ice freeboards from CryoSat-2 and
617 ICESat-2: An exploratory analysis, *Advances in Space Research*, 62, 1243–1250, <https://doi.org/10.1016/j.asr.2017.09.007>,
618 2018.

619 Kwok, R., Cunningham, G., Hancock, D., Ivanoff, A., and Wimert, J.: Algorithm Theoretical Basis Document (ATBD) For
620 Sea Ice Products, 2018.

621 Kwok, R., Kacimi, S., Markus, T., Kurtz, N. T., Studinger, M., Sonntag, J. G., Manizade, S. S., Boisvert, L. N., and Harbeck,
622 J. P.: ICESat-2 Surface Height and Sea Ice Freeboard Assessed With ATM Lidar Acquisitions From Operation IceBridge,
623 *Geophysical Research Letters*, 46, 11228–11236, <https://doi.org/10.1029/2019GL084976>, 2019.

624 Kwok, R., Bagnardi, M., Petty, A., and Kurtz, N.: ICESat-2 sea ice ancillary data - Mean Sea Surface Height Grids,
625 <https://doi.org/10.5281/zenodo.4294048>, 2020.

626 Kwok, R., Petty, A. A., Bagnardi, M., Kurtz, N. T., Cunningham, G. F., Ivanoff, A., and Kacimi, S.: Refining the sea surface
627 identification approach for determining freeboards in the ICESat-2 sea ice products, *The Cryosphere*, 15, 821–833,
628 <https://doi.org/10.5194/tc-15-821-2021>, 2021.

629 Kwok, R., Petty, A., Bagnardi, M., Wimert, J. T., Cunningham, G. F., Hancock, D. W., Ivanoff, A., and Kurtz, N.: Ice, Cloud,
630 and Land Elevation Satellite (ICESat-2) Project Algorithm Theoretical Basis Document (ATBD) for Sea Ice Products, version
631 6, <https://doi.org/10.5067/9VT7NJWOTV3I>, 2023.

632 Lam, H-M., Geldsetzer, T., Howell, S.E.L., and Yackel, J. Snow Depth on Sea Ice and on Land in the Canadian Arctic from
633 Long-Term Observations, *Atmosphere-Ocean*, 61:4, 217-233, <https://doi.org/10.1080/07055900.2022.2060178>, 2023.

634 Landy, J. C., Petty, A. A., Tsamados, M., and Stroeve, J. C.: Sea Ice Roughness Overlooked as a Key Source of Uncertainty
635 in CryoSat-2 Ice Freeboard Retrievals, *Journal of Geophysical Research: Oceans*, 125, e2019JC015820,
636 <https://doi.org/10.1029/2019JC015820>, 2020.

637 Laxon, S. W., Giles, K. A., Ridout, A. L., Wingham, D. J., Willatt, R., Cullen, R., Kwok, R., Schweiger, A., Zhang, J., Haas,
638 C., Hendricks, S., Krishfield, R., Kurtz, N., Farrell, S., and Davidson, M.: CryoSat-2 estimates of Arctic sea ice thickness and
639 volume, *Geophysical Research Letters*, 40, 732–737, <https://doi.org/10.1002/grl.50193>, 2013.

640 Leuschen, C. J., Swift, R. N., Comiso, J. C., Raney, R. K., Chapman, R. D., Krabill, W. B., and Sonntag, J. G.: Combination
641 of laser and radar altimeter height measurements to estimate snow depth during the 2004 Antarctic AMSR-E Sea Ice field
642 campaign, *Journal of Geophysical Research: Oceans*, 113, <https://doi.org/10.1029/2007JC004285>, 2008.

643 Magruder, L. A., Brunt, K. M., and Alonzo, M.: Early ICESat-2 on-orbit Geolocation Validation Using Ground-Based Corner
644 Cube Retro-Reflectors, *Remote Sensing*, 12, 3653, <https://doi.org/10.3390/rs12213653>, 2020.

645 Mahoney, A., Gearheard, S., Oshima, T., and Qillaq, T.: Sea Ice Thickness Measurements from a Community-Based
646 Observing Network, *Bulletin of the American Meteorological Society*, 90, 370–378,
647 <https://doi.org/10.1175/2008BAMS2696.1>, 2009.

648 Maykut, G. A. and Untersteiner, N.: Some results from a time-dependent thermodynamic model of sea ice, *Journal of*
649 *Geophysical Research (1896-1977)*, 76, 1550–1575, <https://doi.org/10.1029/JC076i006p01550>, 1971.

650 Meier, W. and Stroeve, J.: An Updated Assessment of the Changing Arctic Sea Ice Cover, *Oceanog*,
651 <https://doi.org/10.5670/oceanog.2022.114>, 2022.

652 Melling, H.: Sea ice of the northern Canadian Arctic Archipelago, *Journal of Geophysical Research: Oceans*, 107, 2-1-2–21,
653 <https://doi.org/10.1029/2001JC001102>, 2002.

654 Moran, P.A.P.: The interpretation of statistical maps, *Journal of the Royal Statistical Society*, 10, 243-251.

655 Mundy, C. J., Barber, D. G., and Michel, C.: Variability of snow and ice thermal, physical and optical properties pertinent to
656 sea ice algae biomass during spring, *Journal of Marine Systems*, 58, 107–120, <https://doi.org/10.1016/j.jmarsys.2005.07.003>,
657 2005.

658 Moon, W., Nandan, V., Scharien, R. K., Wilkinson, J., Yackel, J. J., Barrett, A., Lawrence, I., Segal, R. A., Stroeve, J.,
659 Mahmud, M., Duke, P. J., and Else, B.: Physical length scales of wind-blown snow redistribution and accumulation on
660 relatively smooth Arctic first-year sea ice, *Environ. Res. Lett.*, 14, 104003, <https://doi.org/10.1088/1748-9326/ab3b8d>, 2019.

661 Nandan, V., Geldsetzer, T., Yackel, J., Mahmud, M., Scharien, R., Howell, S., King, J., Ricker, R., and Else, B.: Effect of
662 Snow Salinity on CryoSat-2 Arctic First-Year Sea Ice Freeboard Measurements, *Geophysical Research Letters*, 44, 10,419-
663 10,426, <https://doi.org/10.1002/2017GL074506>, 2017.

664 Nandan, V., Scharien, R. K., Geldsetzer, T., Kwok, R., Yackel, J. J., Mahmud, M. S., Rösel, A., Tonboe, R., Granskog, M.,
665 Willatt, R., Stroeve, J., Nomura, D., and Frey, M.: Snow Property Controls on Modeled Ku-Band Altimeter Estimates of First-
666 Year Sea Ice Thickness: Case Studies From the Canadian and Norwegian Arctic, *IEEE Journal of Selected Topics in Applied*
667 *Earth Observations and Remote Sensing*, 13, 1082–1096, <https://doi.org/10.1109/JSTARS.2020.2966432>, 2020.

668 Neumann, T. A., Martino, A. J., Markus, T., Bae, S., Bock, M. R., Brenner, A. C., Brunt, K. M., Cavanaugh, J., Fernandes, S.
669 T., Hancock, D. W., Harbeck, K., Lee, J., Kurtz, N. T., Luers, P. J., Luthcke, S. B., Magruder, L., Pennington, T. A., Ramos-
670 Izquierdo, L., Rebold, T., Skoog, J., and Thomas, T. C.: The Ice, Cloud, and Land Elevation Satellite – 2 mission: A global
671 geolocated photon product derived from the Advanced Topographic Laser Altimeter System, *Remote Sensing of Environment*,
672 233, 111325, <https://doi.org/10.1016/j.rse.2019.111325>, 2019.

673 Raney, R. K. and Leuschen, C.: Technical Support for the Deployment Of Radar and Laser Altimeters during LaRA 2002,
674 Final Report, 21, 2003.

675 Ricker, R., Hendricks, S., Helm, V., Skourup, H., and Davidson, M.: Sensitivity of CryoSat-2 Arctic sea-ice freeboard and
676 thickness on radar-waveform interpretation, *The Cryosphere*, 8, 1607–1622, <https://doi.org/10.5194/tc-8-1607-2014>, 2014.

677 Ricker, R., Fons, S., Jutila, A., Hutter, N., Duncan, K., Farrell, S. L., Kurtz, N. T., and Fredensborg Hansen, R. M.: Linking
678 scales of sea ice surface topography: evaluation of ICESat-2 measurements with coincident helicopter laser scanning during
679 MOSAiC, *The Cryosphere*, 17, 1411–1429, <https://doi.org/10.5194/tc-17-1411-2023>, 2023.

680 Rotermund, L. M., Williams, W. J., Klymak, J. M., Wu, Y., Scharien, R. K., and Haas, C.: The Effect of Sea Ice on Tidal
681 Propagation in the Kitikmeot Sea, Canadian Arctic Archipelago, *Journal of Geophysical Research: Oceans*, 126,
682 e2020JC016786, <https://doi.org/10.1029/2020JC016786>, 2021.

683 Tilling, R. L., Ridout, A., and Shepherd, A.: Estimating Arctic sea ice thickness and volume using CryoSat-2 radar altimeter
684 data, *Advances in Space Research*, 62, 1203–1225, <https://doi.org/10.1016/j.asr.2017.10.051>, 2018.

685 Ullaby, F. T., Moore, R. K., and Fung, A. K.: Microwave Remote Sensing. Active and Passive., Geological Magazine, 124,
686 88–88, <https://doi.org/10.1017/S0016756800015831>, 1987.

687 Warren, S. G., Rigor, I. G., Untersteiner, N., Radionov, V. F., Bryazgin, N. N., Aleksandrov, Y. I., and Colony, R.: Snow
688 Depth on Arctic Sea Ice, Journal of Climate, 12, 1814–1829, <https://doi.org/10.1175/1520->
689 0442(1999)012<1814:SDOASI>2.0.CO;2, 1999.

690 Webster, M., Gerland, S., Holland, M., Hunke, E., Kwok, R., Lecomte, O., Massom, R., Perovich, D., and Sturm, M.: Snow
691 in the changing sea-ice systems, Nature Clim Change, 8, 946–953, <https://doi.org/10.1038/s41558-018-0286-7>, 2018.

692 Webster, M. A., Rigor, I. G., Nghiem, S. V., Kurtz, N. T., Farrell, S. L., Perovich, D. K., and Sturm, M.: Interdecadal changes
693 in snow depth on Arctic sea ice, Journal of Geophysical Research: Oceans, 119, 5395–5406,
694 <https://doi.org/10.1002/2014JC009985>, 2014a.

695 Willatt, R., Laxon, S., Giles, K., Cullen, R., Haas, C., and Helm, V.: Ku-band radar penetration into snow cover on Arctic sea
696 ice using airborne data, Ann. Glaciol., 52, 197–205, <https://doi.org/10.3189/172756411795931589>, 2011.

697 Xu, C., Mikhael, W., Myers, P. G., Else, B., Sims, R. P., and Zhou, Q.: Effects of Seasonal Ice Coverage on the Physical
698 Oceanographic Conditions of the Kitikmeot Sea in the Canadian Arctic Archipelago, Atmosphere-Ocean, 59, 214–232,
699 <https://doi.org/10.1080/07055900.2021.1965531>, 2021.

700 Yackel, J., Geldsetzer, T., Mahmud, M., Nandan, V., Howell, S. E. L., Scharien, R. K., and Lam, H. M.: Snow Thickness
701 Estimation on First-Year Sea Ice from Late Winter Spaceborne Scatterometer Backscatter Variance, Remote Sens., 11, 417,
702 <https://doi.org/10.3390/rs11040417>, 2019.

703 Zheng, J., Geldsetzer, T., and Yackel, J.: Snow thickness estimation on first-year sea ice using microwave and optical remote
704 sensing with melt modelling, Remote Sens. Environ., 199, 321–332, <https://doi.org/10.1016/j.rse.2017.06.038>, 2017.

705
706
707
708
709
710
711
712
713
714
715
716

717 **Appendix A**718 **Table A1: Geophysical corrections applied on the IS2 ATL07 product. The range represents the typical variation in the corrections**
719 **as reported in the IS2 Algorithm Theoretical Basis Document (ATBD).**

Geophysical Correction	Typical Range	Source
Solid Earth Tide	-19 to +27 cm	IERS 2010 (Applied in ATL03)
Solid Earth Pole Tides	-0.6 to +0.7 cm	IERS 2010 (Applied on ATL03)
Ocean Pole tides	+/- 2 mm	IERS 2010 (Applied in ATL03)
Ocean loading	-9.7 to +9.3 cm	GOT4.8 Ocean Tide Model (Applied in ATL07)
Ocean Tides	-6.2 to +6.2 m	GOT4.8 Ocean Tide Model (Applied in ATL07)
Long period equilibrium tides	-7.1 to +6.0 cm	GOT4.8 Ocean Tide Model (Applied in ATL07)
Inverted barometer	-53 to +94 cm	ATL09/GEOS5 FP-IT (Applied in ATL07)

720

721 **Appendix B**722 **Table B1: Geophysical Corrections applied in the CS2 Level 2 product. The typical range values are reported in the Cryosat-2**
723 **Baseline E Level 2 Product Handbook.**
724

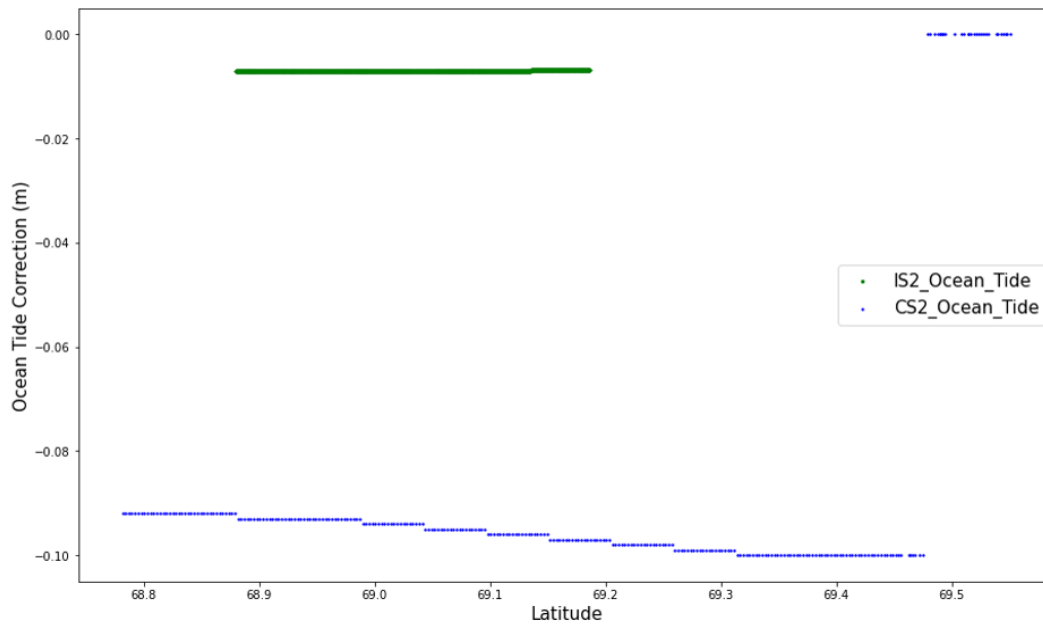
Geophysical Correction	Typical Range	Source
Ocean Tide	-50 to +50 cm	Finite Element Solution FES 2004 Tide Model
Long-Period Equilibrium Ocean Tide	< 1cm	Finite Element Solution FES 2004 Tide Model
Ocean Loading	-2 to +2 cm	Finite Element Solution FES 2004 Tide Model
Solid Earth Tide	-30 to +30 cm	Cartwright Tide model (Cartwright & Edden, 1973)
Geocentric Polar Tide	-2 to +2 cm	Historical Pole Positions from CNES
Inverted Barometer	-15 to +15 cm	Dynamic Surface Pressure from Meteo France

725

726 **Appendix C**

727

728

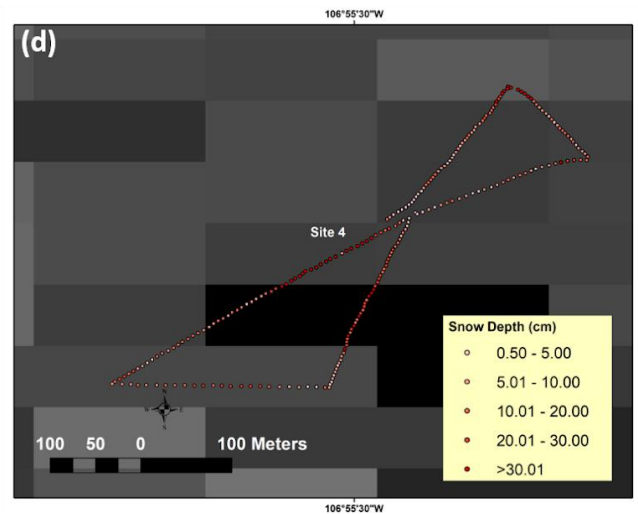
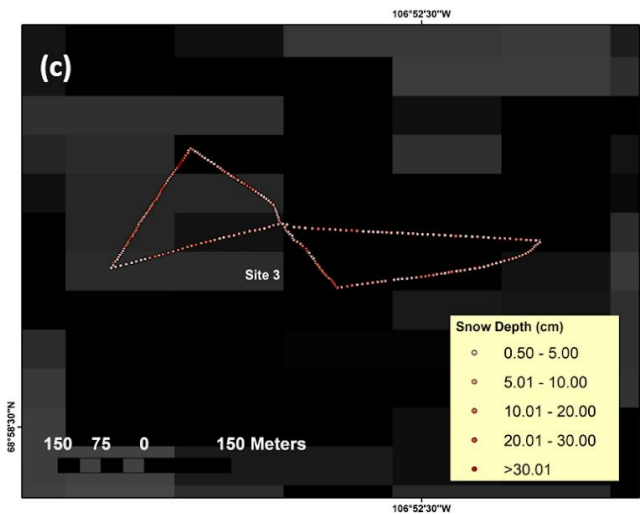
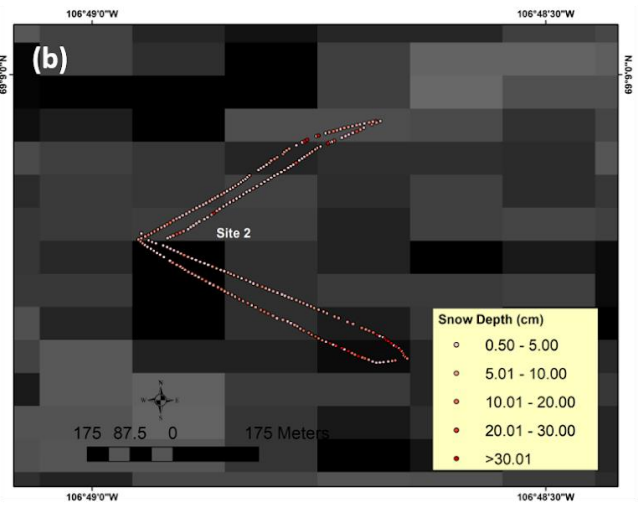
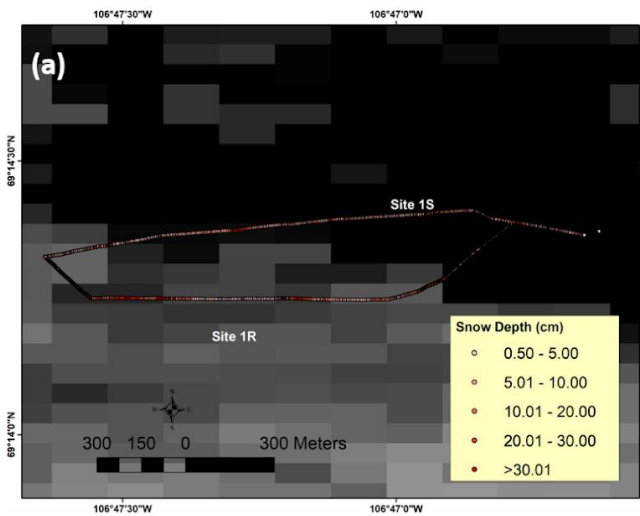


729

730 **Figure C1: Ocean tidal correction used in the IS2 and CS2 tracks. The IS2 ocean tide corrections are shown in green while the CS2**
 731 **ocean tide corrections are shown in blue.**

732 **Appendix D**

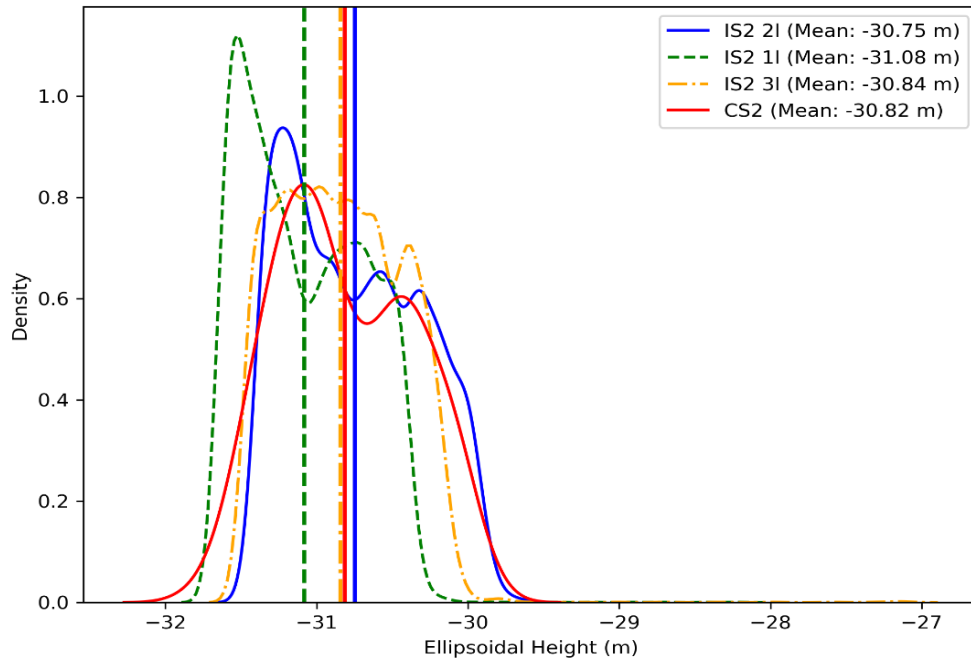
733



734
 735
 736 Figure D1: The in-situ snow depth transects conducted in (a) Site 1 (b) Site 2 (c) Site 3 and (d) Site 4. The spatial
 737 distribution of the snow depths are included for each site.

745

746 **Appendix E**



747

748 Figure E1: ATL07 ICESat-2 strong beam (IS2 1I, 2I, 3I) sea ice height ellipsoidal height distributions compared to the CS2
749 height ellipsoidal height distribution.

750

751

752

753

754

755

756

757

758

759

760

761

763 **Table F1 In-situ versus Cryo2Ice snow depth distribution statistics retrieved using 300 meter averaged IS2 and CS2 height**

		Mean (cm)	Median (cm)	Lower Quartile (cm)	Upper Quartile (cm)	Inter-quartile range (cm)
Site 1	In-Situ	12.2	7.8	4.1	16.3	12.2
	Cryo2Ice	4.7	4.9	-1.8	9.8	11.6
Site 2	In-Situ	9.7	5.2	3.7	9.2	5.5
	Cryo2Ice	1.9	4.8	-5.9	8.5	14.4
Site 3	In-Situ	8.9	6.9	4.2	11.9	7.7
	Cryo2Ice	0.61	3.4	-5.4	5.8	11.2
Site 4	In-Situ	17.1	13.8	6.7	22.4	15.7
	Cryo2Ice	10.6	8.3	-0.6	18.5	19.1

764

765

766 **Table F2 In-situ versus Cryo2Ice snow depth distribution statistics retrieved using 1-km averaged IS2 and CS2 height**

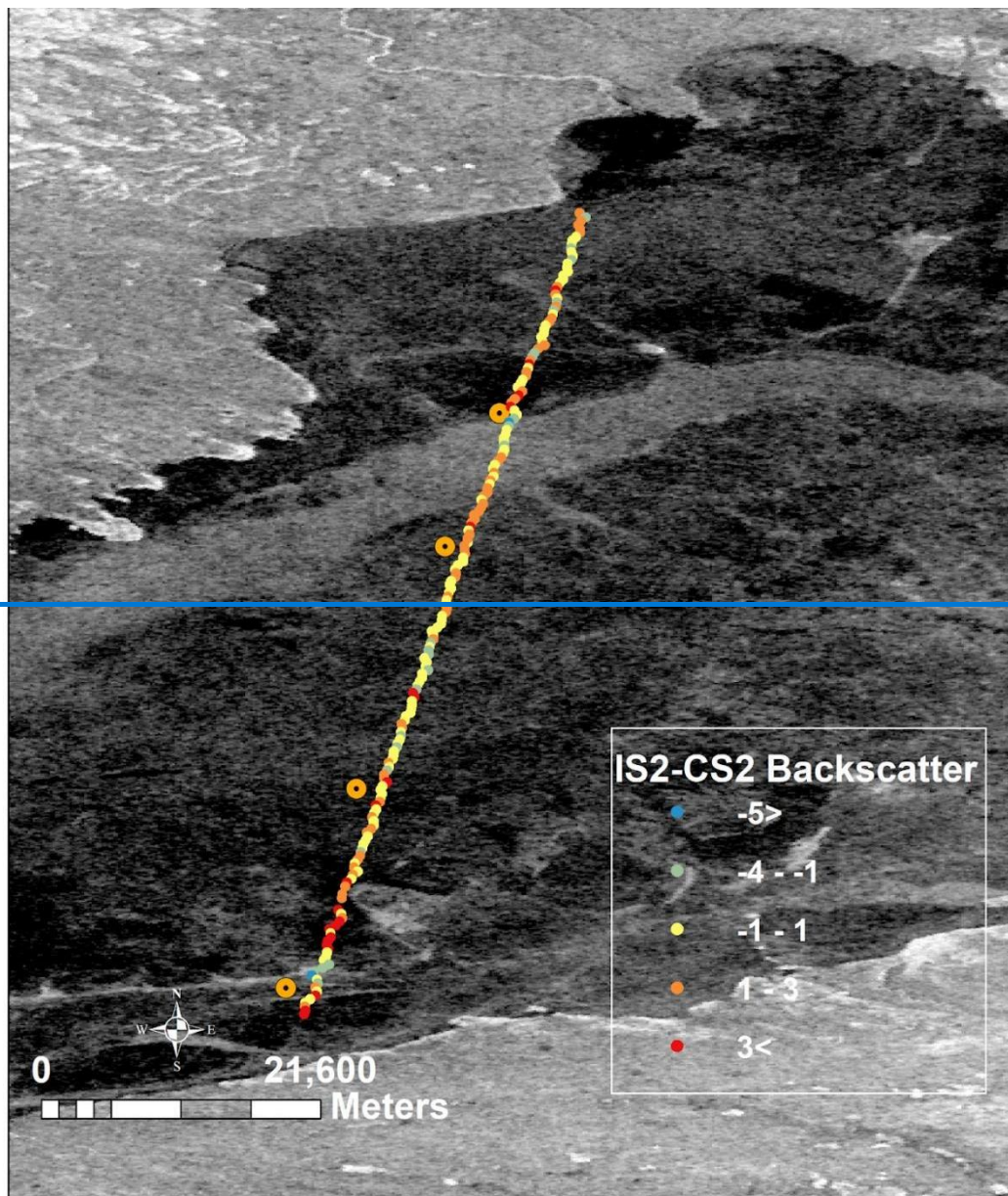
		Mean (cm)	Median (cm)	Lower Quartile (cm)	Upper Quartile (cm)	Inter-quartile range (cm)
Site 1	In-Situ	12.2	7.8	4.1	16.3	12.2
	Cryo2Ice	7.1	6.3	4.6	8.8	4.2
Site 2	In-Situ	9.7	5.2	3.7	9.2	5.5
	Cryo2Ice	4.0	4.9	-8.4	8.2	16.6
Site 3	In-Situ	8.9	6.9	4.2	11.9	7.7
	Cryo2Ice	6.5	2.3	-1.7	3.8	5.5

Site 4	In-Situ	17.1	13.8	6.7	22.4	15.7
	Cryo2I ce	18.7	8.3	15.1	24.2	9.1

767

768

Appendix G



769

770 ~~Figure G1 Spatial Distribution of the backscatter between IS2 and CS2 retrieved from collocated Sentinel-1 image from 5th~~
771 ~~May 2022~~
772